

UCLA

UCLA Previously Published Works

Title

Whole genome sequencing identifies structural variants contributing to hematologic traits in the NHLBI TOPMed program

Permalink

<https://escholarship.org/uc/item/1x35v4cx>

Journal

Nature Communications, 13(1)

ISSN

2041-1723

Authors

Wheeler, Marsha M

Stilp, Adrienne M

Rao, Shuquan

et al.

Publication Date

2022

DOI

10.1038/s41467-022-35354-7

Peer reviewed

Whole genome sequencing identifies structural variants contributing to hematologic traits in the NHLBI TOPMed program

Received: 21 December 2021

Accepted: 29 November 2022

Published online: 08 December 2022

 Check for updates

A list of authors and their affiliations appears at the end of the paper

Genome-wide association studies have identified thousands of single nucleotide variants and small indels that contribute to variation in hematologic traits. While structural variants are known to cause rare blood or hematopoietic disorders, the genome-wide contribution of structural variants to quantitative blood cell trait variation is unknown. Here we utilized whole genome sequencing data in ancestrally diverse participants of the NHLBI Trans Omics for Precision Medicine program ($N = 50,675$) to detect structural variants associated with hematologic traits. Using single variant tests, we assessed the association of common and rare structural variants with red cell-, white cell-, and platelet-related quantitative traits and observed 21 independent signals (12 common and 9 rare) reaching genome-wide significance. The majority of these associations ($N = 18$) replicated in independent datasets. In genome-editing experiments, we provide evidence that a deletion associated with lower monocyte counts leads to disruption of an *SIPR3* monocyte enhancer and decreased *SIPR3* expression.

Structural variants (SVs) are an important, yet under-studied type of human genetic variation. Numerous studies have implicated SVs (defined as > -50 bp) with human diseases as well as normal phenotypic variation^{1–5}. Common SVs (MAF $> 1\%$) are enriched among loci identified in genome-wide association studies (GWAS)⁶. In non-coding regions, SVs have a greater impact on gene expression compared to single nucleotide variants (SNVs) and small insertions and deletions (indels)⁷. However, the discovery and genotyping of SVs is challenging and has lagged behind that of SNVs and indels. Many SVs are located within repetitive regions of the genome and often have complex structures including multiallelic copy number or repeat expansion, deletions with multiple breakpoints, or repeated rearrangement or complex inversions⁶. As a result, the contribution of SVs to the genetic architecture of complex traits remains poorly characterized.

The recent application of ensemble detection methods to whole genome sequencing (WGS) projects, particularly to large, multi-ancestry datasets, provides an opportunity to characterize the

contribution of common and rare SVs to complex traits. Towards this end, we have utilized SVs detected from high-coverage WGS data from the NHLBI Trans-Omics for Precision Medicine (TOPMed) program and characterized their relationship to quantitative blood cell traits.

Red blood cell (RBC), white blood cell (WBC), and platelet laboratory parameters are routinely measured in clinical laboratories and used for monitoring general health status and diagnosis of acquired and inherited blood-related disorders. In the general population, hematologic quantitative traits are highly heritable and serve as a model system for studying the genetic architecture of complex traits⁸. Thus far, hundreds of genomic loci and thousands of genetic variants have been associated with hematologic traits; however, these variants are almost exclusively SNVs and indels^{9,10}. For a few GWAS loci, there is evidence that common SVs are likely the causal variant responsible for the phenotypic effects in the population at large. For example, a common 3.7 kb alpha-globin gene deletion largely accounts for the strong association signal between RBC phenotypes and the

 e-mail: pauer@mcw.edu; apreiner@uw.edu

16p13.3 locus in African ancestry populations^{11–13}. While private SVs have been identified in individuals with rare Mendelian blood disorders (for example, a rare *PLAU* 78 kb tandem duplication responsible for autosomal dominant Quebec platelet disorder¹⁴), the contribution of rare SVs (MAF < 1%) to quantitative hematologic traits among unselected individuals has not been assessed.

In up to 50,675 ancestrally diverse TOPMed participants, we assessed the association of common and rare SVs (deletions, duplications, and inversions) with variation in RBC, WBC, and platelet-related quantitative traits. We characterized linkage disequilibrium patterns and performed conditional regression analyses that included SNVs/indels previously associated with the same hematologic trait. Additionally, we used gene editing in monocytic and primary human hematopoietic stem and progenitor cells (HSPCs) followed by xenotransplantation to demonstrate the mechanism by which a newly detected deletion disrupts an *SIPR3* monocyte enhancer and leads to decreased *SIPR3* expression and lower monocyte count.

Results

Identification of common and rare SVs associated with blood cell traits

We performed single variant association tests, across 24 quantitative hematologic traits in up to 50,675 multi-ancestry TOPMed participants (Supplementary Data 1). Single variant association tests were performed for SVs with a minor allele count (MAC) ≥ 5 (number of SVs = 96,049). SVs in TOPMed were detected and genotyped from WGS using the Parliament2 pipeline¹⁵ and muCNV genotyper¹⁶ (see Methods). The QQ plots and genomic inflation factors (ranging from 0.981 to 1.056) were well-calibrated indicating good control of population stratification and relatedness (Fig. S1). Further stratification of the QQ plots by allele frequency showed no evidence of inflation even for minor allele counts in the 5–10 range (Fig. S2). Across the 24 hematologic traits, a total of 21 independent SVs (deletions = 14, duplications = 6, and inversions = 1) or 41 SV-trait associations were genome-wide significant (Table 1 and Fig. S3).

The 21 trait-associated SVs ranged in size from -60 bp to >160 kb (Table 1) and exhibited a range of allele frequencies: 12 are common (overall TOPMed MAF > 1%) and 9 are rare (ranging from 0.006% to 0.7% MAF in TOPMed) with a few significant SVs exhibiting allele frequencies differences across populations (Table 1). For instance, the monocyte-associated deletion on chromosome 9q22.1 and a subset of the 16p13.3 red cell trait-associated SVs are more common in individuals of African ancestry than in individuals of non-African ancestry.

Replication of significant SV-blood cell trait associations

We attempted replication for each of the 21 trait-associated SVs using a combination of short-read and long-read WGS data and genotype imputation. We utilized independent datasets composed of Icelandic (deCODE genetics)^{17–19} and multi-ancestry (UK Biobank, UKBB)²⁰ participants. Note that the SV calling and genotyping algorithms used in replication datasets (described under Methods) are different from the Parliament2 pipeline used for SV discovery in TOPMed. To account for these methodological differences, we determined a set of “representative SVs” in deCODE genetics and UKBB datasets. We defined an SV in a replication dataset as “representative” if the SV was located within 5 kb of the trait-associated TOPMed SV and if the two SV sizes overlapped by at least 25%. In addition, we considered SVs as representative if they were the same structural variant type (e.g. both SVs were deletions) and had similar minor allele frequencies in the relevant population.

Using these criteria, 3 of the 21 trait-associated SVs did not have a SV representative in deCODE or UKBB datasets, including SVs at 2q11.2 (2:88832769–88860930), 3q22.1 (3:133621201–133784900), and 17p11.2 (17:21659501–21795800) (Supplementary Data 2). A total of 18

trait-associated SVs did have a representative and all of these were robustly replicated for the same blood cell trait (i.e., with a p -value < 0.05/number of its representative SVs in deCODE Icelandic, UKBB British, UKBB African, or UKBB South Asian cohorts and consistent direction of the effect) (Supplementary Data 2).

Trait-associated SVs in regions of LD with known GWAS loci

To determine if trait-associated SVs discovered in TOPMed are independent of previously reported GWAS SNVs/indels^{9,10,21–23}, we calculated pairwise linkage disequilibrium (LD) between TOPMed SVs and TOPMed SNVs/indels (Table 2, Fig. S4). We also performed two sets of conditional analyses (see Methods). LD analysis shows 16 of 21 trait-associated SVs are in at least moderate LD ($r^2 \geq 0.75$) with one SNV/indel previously associated with the same hematologic trait (Table 2, Fig. S4). These include 7 SVs with at least one trait-associated SNV/indel in near perfect LD ($r^2 \geq 0.99$). Conditional regression analysis confirmed that 16 SV association signals were not significant following adjustment for known SNV/indels at the same trait loci (Table 3), supporting the non-independence between SV and SNV/indel associations at these loci.

Conditional analyses of trait-associated SVs adjusting for known GWAS SNVs/indels

A total of 5 trait-associated SVs remained genome-wide significant following conditional analyses (Table 3). This result suggests that these association SV signals may be causally distinct and that the previously identified association with an SNV/indel was reported due to LD with the unmeasured causal SV. These 5 SVs span 4 genomic loci. We discuss these genomic loci in greater detail below.

16p13.3 (alpha-globin) locus. The strongest association signal in our analyses was located at the 16p13.3 locus where a deletion spanning *HBA1/HBA2* (16:172001–177200) was associated with all 7 red cell traits (Table 1, Fig. S5). LD and conditional analyses indicate this deletion (16:172001–177200) is independent of other known red cell trait-associated SNVs/indels (Tables 2, 3). Although Parliament2 predicted this deletion as being 5.2 kb in size (see Table 1), this deletion represents a previously characterized 3.7 kb alpha-globin deletion¹¹. This was confirmed by WGS read visualization in samples predicted to exhibit the *HBA1/HBA2* (16:172001–177200) deletion. Visualization shows SV breakpoints predicted by Parliament2 for this event are inaccurate and span the previously characterized 3.7 kb deletion (see example in Fig. S5). The 3.7 kb alpha-globin deletion is known to be more common in African ancestry individuals²¹. In our study, the overall allele frequency of the *HBA1/HBA2* deletion (16:172001–177200) was 5.7% and 17.6% in the African ancestry sub-population.

SV analyses also found the *HBA1/HBA2* deletion (16:172001–177200) as significantly associated with higher mean platelet volume (MPV) (Table 1). This was unexpected as none of the alpha-globin genes are known to regulate megakaryocyte or platelet production. While transcripts of genes located within the alpha-globin cluster on 16p13.3 are detectable in iPSC-induced megakaryocytes²⁴, we observed no evidence that this deletion is a *cis*-eQTL among African-ancestry individuals from the TOPMed GeneSTAR cohort (Bonferroni-corrected P -values > 0.15 for all genes within a 1 Mb window). These observations are based on evidence from analysis of RNA from platelets ($n = 110$) and iPSC-induced megakaryocytes ($n = 84$). Relatedly, we found no association between the alpha-globin deletion (16:172001–177200) and circulating platelet counts in TOPMed ($P = 0.75$). Based on these observations, along with the lack of any apparent association of the 16:172001–177200 deletion with circulating platelet count in TOPMed ($P = 0.75$), we hypothesize that the association with platelet size likely represents a laboratory artifact in which very small (microcytic) RBCs are being counted as “large platelets” thereby resulting in an apparent increase in MPV.

Table 1 | Summary of genome-wide structural variants associated with hematological trait

Gene(s)	Locus	SV Breakpoints ¹	SV type ²	Length (bp)	TOPMed Allele Frequencies					Significant single variant association tests			
					Overall	African ³	Asian ³	Hispanic ³	European ³	Significant Trait	Effect Estimate	SE	P-value
-	2p11.2 ⁴	2:88832769-88860930	DEL	28162	1.98E-04	4.06E-05	0	0	2.98E-04	Lymphocytes	1.878	0.310	1.36E-09
RAB7A	3q21.3	3:128694260-128695207	DUP	948	0.085	0.022	0.031	0.065	0.119	Monocyte prop.	2.813	0.426	3.84E-11
SRPRB, TF, TOPBP1	3q22.1	3:133621201-133784900	DUP	163700	0.208	0.141	0.308	0.200	0.236	TIBC	20.809	2.209	4.56E-21
C5orf36, LINC02000, RAB6B, SLCO2A1, SRPRB, TF	3q22.1-q22.2	3:133786201-134102300	DUP	316100	0.272	0.207	0.358	0.267	0.292	UIBC	19.298	2.553	4.09E-14
PSORS1C1	6p21.33	6:31132409-31132465	DEL	57	0.085	0.049	0.075	0.103	0.094	TIBC	17.804	2.324	1.84E-14
-	6p21.32	6:32591559-32591660	DEL	102	0.264	0.167	0.281	0.293	0.293	UIBC	19.463	2.687	4.35E-13
-	6p21.1	6:41897089-41897626	DEL	538	0.183	0.079	0.209	0.151	0.235	Lymphocytes	0.075	0.012	2.01E-09
										WBC	0.092	0.015	1.25E-09
										MCH	-0.187	0.022	1.28E-17
										MCV	-0.595	0.055	3.04E-27
										RBC	0.033	0.005	1.57E-12
CCND3	6p21.1	6:41985574-41988887	DEL	3314	0.007	0.002	0.001	0.007	0.010	MCV	1.556	0.256	1.16E-09
-	6p23.3	6:134878573-134878641	DUP	69	0.044	0.072	0.030	0.037	0.036	MCH	-0.254	0.046	4.23E-08
-	9q22.1	9:88923551-88924152	DEL	602	0.034	0.117	7.08E-04	0.032	7.31E-04	Monocytes	-0.029	0.004	2.20E-11
										Monocyte prop.	-0.004	-0.004	1.07E-12
ATXN2	12q24.12	12:111538485-111542205	DEL	3721	0.068	0.016	0.021	0.058	0.092	Platelets	-6.063	0.820	1.40E-13
ATXN2	12q24.12	12:111542097-111542205	INV	109	0.062	0.015	0.021	0.054	0.085	Platelets	-6.371	0.911	2.65E-12
-	14q32.33 ⁴	14:105863184-105897962	DEL	34779	2.24E-04	4.16E-05	0	0	3.43E-04	Lymphocytes	2.037	0.256	1.87E-15
										Lymphocyte prop.	0.228	0.030	2.49E-14
										Neutrophil prop.	-0.222	0.034	1.08E-10
-	14q32.33 ⁴	14:105864247-105902650	DEL	38404	7.96E-05	0	0	0	1.41E-04	WBC	3.115	0.483	1.15E-10
HBA1, HBA2	16p13.3	16:165396-184701	DEL	19306	5.95E-05	0	0.004	6.32E-05	0	MCH	-6.570	0.865	3.12E-14
										MCV	-16.599	2.305	5.97E-13
										RBC	1.437	0.189	3.02E-14
HBA1, HBA2	16p13.3	16:172001-177200	DEL	5200	0.057	0.176	0.030	0.060	0.008	Hematocrit	-0.485	0.054	2.65E-19
										Hemoglobin	-0.437	0.018	5.06E-127
										MCH	-2.668	0.038	<5E-324
										MCHC	-0.701	0.015	<5E-324
										MCV	-6.276	0.099	<5E-324
										RBC	0.296	0.008	<5E-324
										RBW	0.545	0.030	1.19E-73
										MPV	0.118	0.021	1.60E-08
FAM234A	16p13.3	16:246437-249971	DEL	3535	0.006	0.019	7.39E-04	0.005	7.54E-05	MCH	-0.788	0.120	4.90E-11
										MCV	-1.917	0.310	6.07E-10

Table 1 (continued) | Summary of genome-wide structural variants associated with hematological trait

Gene(s)	Locus	SV Breakpoints ¹	SV type ²	Length (bp)	TOPMed Allele Frequencies					Significant single variant association tests			
					Overall	African ³	Asian ³	Hispanic ³	European ³	Significant Trait	Effect Estimate	SE	P-value
CAPN15	16p13.3	16:550075-550141	DEL	67	0.025	0.116	7.05E-04	0.020	3.39E-04	MCH	-0.374	0.063	2.92E-09
KCNJ18	17p11.2	17:21659501-21795800	DUP	136300	0.511	0.519	0.509	0.508	0.508	MCV	-0.929	0.162	8.74E-09
-	18p11.22	18:9621931-9622237	DEL	307	0.791	0.839	0.921	0.766	0.770	Lymphocyte prop. Neutrophils prop.	0.022	0.004	4.36E-10
TMPRSS6	22q12.3	22:37067818-37067888	DUP	71	0.947	0.483	0.323	0.324	0.301	MPV	-0.079	0.014	9.32E-09
										Hemoglobin	0.059	0.010	1.62E-08

¹Structural variant breakpoints predicted by the Parliament2 pipeline.

²Types of structural variant identified: deletions (DEL), duplications (DUP), inversions (INV).

³Discrete ancestry subgroups are based on genetically inferred ancestry and a machine learning algorithm that refines self-identified ancestry.

⁴Based on location and WGS read visualization SV likely represents a somatic deletion or a complex rearrangement due to V(D)J recombination events.

All *p*-values are derived from two-sided *t*-tests and are not adjusted for multiple comparisons. WBC White Blood Cells, TIBC Total iron binding capacity, UIBC Unsaturated iron binding capacity, MCH Mean corpuscular hemoglobin, MCV Mean corpuscular volume, RBC Red blood cells, RBW Red cell width, MCHC Mean corpuscular hemoglobin concentration, MPV Mean Platelet Volume.

In addition to the *HBA1/HBA2* deletion (16:172001-177200), analyses identified 3 other 16p13.3 deletions located within 500 kb of the alpha-globin gene cluster. LD and conditional analyses suggest these 3 deletions are not independent from trait-associated SNVs/indels in this region (Tables 2, 3). However, all 3 deletions showed a similar “thalassemia-like” pattern of red cell phenotypic association (lower MCH and MCV and higher RBC count) (Table 1)¹¹. These deletions range in size from -70 bp to 19,000 bp. The -19 kb deletion (allele frequency 0.006% in TOPMed overall and 0.4% in TOPMed Asian ancestry individuals) impacts both *HBA1* and *HBA2* and likely corresponds to the well-characterized alpha-thalassemia variant known as -(SEA)¹¹. The two other red cell trait-associated SVs on 16p13.3 are located -70 to -400 kb downstream of the alpha-globin genes and are not predicted to alter regions involved in alpha-globin gene regulation or show evidence by promoter Hi-C capture of physical interaction with globin gene promoters in blood cells (Supplementary Data 3).

17p11.2 (*KCNJ18*) locus. A complex, multiallelic SV near the centromere of chromosome 17 (17p11.2) was significantly associated with higher lymphocyte proportions and lower neutrophil proportions (Table 1, Fig. S5). This SV is predicted by Parliament2 to be a large duplication that includes the *KCNJ18* gene. Of note, the genomic region containing *KCNJ18* is not present in GRCh37; thus, this region was not interrogated in prior GRCh37 blood cell trait GWAS. In GRCh38, there is one copy of *KCNJ18*; however, based on Parliament2 SV calls, this region is likely duplicated (diploid copy number = 4) in most individuals (-87% of individuals in our TOPMed dataset). A subset of individuals (-2.7%) are estimated to have more than 4 diploid copies.

There is no LD between the *KCNJ18* SV and SNV/indels in the region (Table 2) and the SV-trait association is independent of known GWAS variants (Table 3). These results are consistent with a recent TOPMed WGS-based analysis, where no SNVs/indels in the 17p11.2 region were associated with WBC, neutrophil, or lymphocyte traits²². However, given the phenotypic pattern (opposing effects on neutrophil and lymphocyte proportions) associated with the *KCNJ18* duplication, the complexity of the locus, the absence of a known role of *KCNJ18* in leukocyte biology, and the lack of detection in our replication cohorts (see above) additional work is needed to substantiate these results.

2p11.2 and 14q32.33 immunoglobulin gene regions. Complex SVs at two loci, 2p11.2 and 14q32.33, were significantly associated with lymphocyte, neutrophil and WBC traits (Table 1, Fig. S5). These SV associations remained significant following adjustment for known WBC trait-associated SNVs/indels (Table 3). SVs at both of these loci are rare and relatively large in size (Table 1). They are predicted to impact immunoglobulin kappa (2p11.2) and heavy chain (14q32.33) gene clusters. Based on their location and on visualization of WGS reads, these SVs likely represent somatic deletions and/or complex rearrangements due to V(D)J recombination events related to B cell maturation or immunoglobulin production²⁵.

Proportion of TOPMed SVs tagging known hematologic trait GWAS sentinel SNV/indels

To more broadly understand the extent to which SVs tag known, blood-cell trait SNVs/indels, we calculated LD for the genotypes of previously-reported SNVs/indels¹⁰ and the genotypes of SVs TOPMed participants. These analyses were performed in European ancestry samples (see Methods). Approximately 3% of previously-reported blood cell trait-associated SNVs/indels¹⁰ (171 of the 6652) were well-tagged ($r^2 > 0.8$) by a TOPMed SV. For these 171 correlated pairs, we compared the trait-association *p*-values in TOPMed in an equivalent sample set of individuals with European ancestry. For most of the SNV/indel-SV pairs, the *p*-values were within an order of magnitude of each

Table 2 | Single nucleotide variants (SNVs) and small insertions and deletions (indels) in linkage disequilibrium ($r^2 \geq 0.75$) with structural variants associated with hematological traits

Gene(s)	Locus	SV Breakpoints ¹	SV type ²	SV allele frequency	SNV/indel; ref>alt	SNV, indel allele frequency	r^2	SNV/indel P-value ³	SNV/indel Effect Estimate ³	SNV/indel Effect Estimate SE ³
-	2p11.2	2:88832769-88860930	DEL	1.98E-04	-	-	-	-	-	-
RAB7A	3q21.3	3:128694260-128695207	DUP	0.085	3:128694296; A>T	0.08	0.781	5.60E-08	-0.002	0.0004
SRPRB, TF, TOPBP1	3q22.1	3:133621201-133784900	DUP	0.208	3:133789620; A>T	0.295	0.819	3.70E-32	17.697	1.499
C3orf36, LINCO2000, RAB6B, SLCO2A1, SRPRB, TF	3q22.1-q22.2	3:133786201-134102300	DUP	0.272	3:133789620; A>T	0.295	0.791	3.70E-32	17.697	1.499
PSORS1C1	6p21.33	6:31132409-31132465	DEL	0.085	6:31133806; G/>A	0.084	0.99	3.15E-06	0.109	0.023
-	6p21.32	6:32591559-32591660	DEL	0.264	6:32593469; T>C	0.277	0.999	1.23E-08	0.084	0.015
-	6p21.1	6:41897089-41897626	DEL	0.183	6:41880062; G>A	0.186	1	3.74E-18	-0.18	0.021
CCND3	6p21.1	6:41985574-41988887	DEL	0.007	6:41984773; T>G	0.007	0.999	4.67E-10	0.613	0.098
-	6p23.3	6:134878573-134878641	DUP	0.044	6:134870213; A>G	0.107	0.79	7.16E-12	-0.189	0.028
-	9q22.1	9:88923551-88924152	DEL	0.034	9:88921159; C>A	0.04	0.996	1.03E-11	-0.029	0.004
ATXN2	12q24.12	12:111538485-111542205	DEL	0.068	12:111599646; G, > A	0.058	0.991	7.81E-14	-6.142	0.822
ATXN2	12q24.12	12:111542097-111542205	INV	0.062	12:111599646; G>A	0.058	0.936	7.81E-14	-6.142	0.822
-	14q32.33	14:105863184-105897962	DEL	2.24E-04	-	-	-	-	-	-
-	14q32.33	14:105864247-105902650	DEL	7.96E-05	-	-	-	-	-	-
HBA1, HBQ1, HBA2	16p13.3	16:165396-184701	DEL	5.95E-05	16:199621; AG>A	0.0004	0.848	7.16E-13	-5.894	0.821
HBA1, HBA2, HBQ1	16p13.3	16:172001-177200	DEL	0.057	-	-	-	-	-	-
FAM234A	16p13.3	16:246437-249971	DEL	0.006	16:244752; G, > A	0.007	0.983	2.39E-11	-0.764	0.114
CAPN15	16p13.3	16:550075-550141	DEL	0.025	16:550141; T>C	0.089	0.857	1.08E-20	-0.333	0.036
KCNJ18	17p11.2	17:21659501-21795800	DUP	0.511	-	-	-	-	-	-
-	18p11.22	18:9621931-9622237	DEL	0.791	18:9621307; T>G	0.781	0.998	1.29E-07	-0.068	0.013
TMPRSS6	22q12.3	22:37067818-37067888	DUP	0.347	22:37071230; C>T	0.438	0.774	1.47E-13	0.125	0.017

¹Structural variant breakpoints predicted by the Parliament2 pipeline.

²Types of structural variant identified: deletions (DEL), duplications (DUP), inversions (INV).

³Single variant association test statistics performed for SNV, indels, performed using the same sample set used for SV analyses and for the same hematological trait(s).

All *p*-values are derived from two-sided *t*-tests and are not adjusted for multiple comparisons.

Table 3 | Structural variants conditioned on single nucleotide variants/indels from previous genome-wide association studies

Gene(s)	Locus	SV Breakpoints	SV type	TOPMed Allele Frequency	Significant Trait	Marginal			Conditioned on TOPMed ¹			Conditioned on BCX ²		
						Effect Estimate	Effect Estimate SE	P-value	Effect Estimate	Effect Estimate SE	P-value	Effect Estimate	Effect Estimate SE	P-value
-	2p11.2 ³	2-88832769-88860930	DEL	1.98E-04	Lymphocytes	1.878	0.31	1.36E-09	1.742	0.288	1.49E-09	2.087	0.309	1.42E-11
RAB7A	3q21.3	3-128694260-128695207	DUP	0.085	Monocyte prop.	-0.002	0.0004	6.91E-09	-0.001	3.93E-04	0.181	-7.31E-04	4.18E-04	0.08
SRPRB, TF, TOPBP1	3q22.1	3-133621201-133784900	DUP	0.208	TIBC	20.809	2.209	4.56E-21	-0.751	2.145	0.726	-	-	-
C3orf36, LINC02000, RAB6B, SLC02A1, SRPRB, TF	3q22.1-q22.2	3-133786201-134102300	DUP	0.272	UIBC	19.298	2.553	4.09E-14	-1.899	3.537	0.591	-	-	-
PSORS1C1	6p21.33	6-31132409-31132465	DEL	0.085	TIBC	17.804	2.324	1.84E-14	-1.179	1.972	0.55	-	-	-
-	6p21.32	6-32591559-32591660	DEL	0.264	UIBC	19.463	2.687	4.35E-13	1.182	3.387	0.727	-	-	-
-	6p21.1	6-41897089-41897626	DEL	0.183	Lymphocytes	0.075	0.012	2.01E-09	0.023	0.029	0.426	0.047	0.014	9.48E-04
CCND3	6p21.1	6-41985574-41988887	DEL	7.00E-03	WBC	0.092	0.015	1.25E-09	0.146	0.061	0.016	0.068	0.016	1.20E-05
-	6p23.3	6-134878573-134878641	DUP	4.40E-02	MCH	-0.254	0.046	4.23E-08	-0.039	0.052	0.449	-0.093	0.045	0.042
-	9q22.1	9-88923551-88924152	DEL	0.034	Monocytes	-0.029	0.004	2.20E-11	0.014	0.029	0.642	-0.032	0.004	4.64E-13
ATXN2	12q24.12	12-111538485-111542205	DEL	0.068	Monocyte prop.	-0.004	0.001	1.07E-12	0.005	0.004	0.222	-0.005	5.89E-04	2.61E-16
ATXN2	12q24.12	12-111542097-111542205	INV	0.062	Platelets	-6.063	0.82	1.40E-13	8.886	7.878	0.259	-1.595	1.046	0.127
-	14q32.33 ³	14-105863184-105897962	DEL	2.24E-04	Platelets	-6.371	0.911	2.65E-12	0.385	2.423	0.874	-1.656	1.108	0.135
HBA1, HBQ1, HBA2	16p13.3	16-165396-184701	DEL	5.95E-05	Lymphocytes	2.037	0.256	1.87E-15	2.76	0.258	1.13E-26	2.248	0.254	9.36E-19
-	14q32.33 ³	14-105863184-105897962	DEL	2.24E-04	Lymphocyte prop.	0.228	0.030	2.49E-14	0.203	0.028	2.31E-13	0.208	0.027	1.71E-14
-	14q32.33 ³	14-105864247-105902650	DEL	7.96E-05	Neutrophils prop.	-0.222	0.034	1.08E-10	-0.207	0.033	6.33E-10	-0.212	0.033	1.52E-10
HBA1, HBQ1, HBA2	16p13.3	16-172001-177200	DEL	0.057	WBC	3.115	0.483	1.15E-10	3.144	0.471	2.51E-11	3.229	0.472	7.52E-12
-	16p13.3	16-165396-184701	DEL	5.95E-05	MCH	-6.57	0.865	3.12E-14	-0.782	2.588	0.762	-6.053	0.808	6.66E-14
HBA1, HBA2, HBQ1	16p13.3	16-172001-177200	DEL	0.057	MCV	-16.599	2.305	5.97E-13	-2.362	6.497	0.716	-15.189	2.151	1.64E-12
-	16p13.3	16-172001-177200	DEL	0.057	RBC	1.437	0.189	3.02E-14	0.622	0.581	0.284	1.359	0.185	1.99E-13
HBA1, HBA2, HBQ1	16p13.3	16-172001-177200	DEL	0.057	Hematocrit	-0.485	0.054	2.65E-19	-0.467	0.053	1.50E-18	-0.492	0.054	5.05E-20
-	16p13.3	16-172001-177200	DEL	0.057	Hemoglobin	-0.437	0.018	5.06E-127	-0.44	0.025	4.87E-71	-0.449	0.021	8.19E-104
-	16p13.3	16-172001-177200	DEL	0.057	MCH	-2.668	0.038	<5E-324	-2.621	0.06	<5E-324	-2.704	0.041	<5E-324
-	16p13.3	16-172001-177200	DEL	0.057	MCHC	-0.701	0.015	<5E-324	-0.652	0.025	5.87E-156	-0.708	0.016	<5E-324
-	16p13.3	16-172001-177200	DEL	0.057	MCV	-6.276	0.099	<5E-324	-6.22	0.153	<5E-324	-6.483	0.111	<5E-324
-	16p13.3	16-172001-177200	DEL	0.057	RBC	0.296	0.008	<5E-324	0.267	0.012	9.77E-109	0.298	0.009	1.58E-245

Table 3 (continued) | Structural variants conditioned on single nucleotide variants/indels from previous genome-wide association studies

Gene(s)	Locus	SV Breakpoints	SV type	TOPMed Allele Frequency	Significant Trait	Marginal			Conditioned on TOPMed ¹			Conditioned on BCX ²		
						Effect Estimate	Effect Estimate SE	P-value	Effect Estimate	Effect Estimate SE	P-value	Effect Estimate	Effect Estimate SE	P-value
					RBW	0.545	0.03	1.19E-73	0.509	0.036	1.79E-46	0.566	0.032	3.52E-70
FAM234A	16p13.3	16:246437-249971	DEL	0.006	MPV	0.118	0.021	1.60E-08	0.119	0.019	6.23E-10	0.117	0.019	5.99E-10
					MCH	-0.788	0.12	4.90E-11	-0.401	0.264	0.129	-0.86	0.116	1.48E-13
					MCV	-1.917	0.31	6.07E-10	-0.502	0.686	0.464	-1.958	0.298	5.41E-11
CAPN5	16p13.3	16:550075-550141	DEL	0.025	MCH	-0.374	0.063	2.92E-09	-0.036	0.072	0.611	-0.412	0.061	1.21E-11
					MCV	-0.929	0.162	8.74E-09	-0.27	0.185	0.144	-0.618	0.155	6.86E-05
KCNJ18	17p11.2	17:21659501-21795800	DUP	0.511	Lymphocyte prop.	0.022	0.004	4.36E-10	0.023	0.003	2.17E-11	0.023	0.003	4.07E-11
					Neutrophils prop.	-0.025	0.004	3.90E-10	-0.024	0.004	1.56E-09	-0.023	0.004	2.57E-09
	18p11.22	18:9621931-9622237	DEL	0.791	MPV	-0.079	0.014	9.32E-09	-0.043	0.031	0.167	-0.065	0.03	0.031
TMPRSS6	22q12.3	22:37067818-37067888	DUP	0.347	Hemoglobin	0.059	0.01	1.62E-08	-0.007	0.016	0.669	-0.006	0.015	0.685

¹Analyses included previously-reported SNVs or small indels with $P < 5 \times 10^{-8}$ in TOPMed single variant association tests (Mikhaylova et al. 2021; Hu et al. 2021).

²Analysis included TOPMed SNVs and small indels that matched variants reported in Chen et al. 2020 and Vuckovic et al. 2020 as part of the Blood Cell Consortium (BCX).

³Based on location and WGS read visualization SV likely represents a somatic deletion or a complex rearrangement due to (VDJ) recombination events. Conditional analyses were performed for each blood trait. Matched variants on each chromosome were LD-pruned and included as fixed effects in a two-stage LMM association testing. All p -values are derived from two-sided t -tests and are not adjusted for multiple comparisons. WBC White Blood Cells, TIBC Total iron binding capacity, UIBC Unsaturated iron binding capacity, MCH Mean corpuscular hemoglobin, MCV Mean corpuscular volume, RBC Red blood cells, RBW Red cell width, MCHC Mean corpuscular hemoglobin concentration, MPV Mean Platelet Volume.

other (Fig. S6), indicating additional functional analyses are needed to identify the causal variant.

Functional annotation of blood cell trait-associated SVs

Functional annotation can provide additional information to prioritize causal variants at trait-associated loci. Of the 21 trait-associated SVs, 7 SVs (4 duplications and 3 deletions) are predicted to overlap coding regions and thus potentially impact protein structure/function (Supplementary Data 3). In addition to the *KCNJ18* SV described above, two duplications spanning the transferrin gene (*TF*) coding and regulatory regions were associated with higher TIBC or transferrin levels (Table 1). Two red cell phenotype-associated deletions are predicted to impact coding regions namely the deletion encompassing the known 3.7 kb alpha-globin deletion which impacts the 3' end of *HBA2* and 5' end of *HBA1* and the 19 kb deletion which comprises the SEA alpha-globin deletion and impacts both alpha-globin genes as well as *HBM* and *HBQ1*.

Based on functional annotation, most trait-associated SVs ($N = 14$) are predicted to only impact non-coding/regulatory genomic regions (intronic=6, intergenic=8) (Supplementary Data 3). We cross-referenced SVs with candidate *cis* regulatory elements (cCREs) from ENCODE and several annotations relevant to 3D chromosome structure (frequently interacting regions or FIREs, topologically associating domains or TADs, super-interactive promoters or SIPs, and chromatin interactions²⁶⁻³¹). Annotation results show 11 trait-associated SVs overlapped cCREs, 11 overlapped with TAD boundaries, and 3 overlapped with FIREs in relevant tissues/cell-types (i.e., GM12878 and spleen) (Supplementary Data 3). Two SVs overlapped SIPs in relevant cell-types. Chromatin interaction annotations from promoter capture Hi-C (pHi-C) data²⁸ show that across 17 blood-cell-lineage cell types, 5 SVs overlap with the promoter regions of 11 genes. This includes deletions which overlap the promoter regions for the gene *HLA-DRB1* and a duplication which overlaps the promoter region of the *TF* gene. pHi-C data also show 10 SVs overlap regions that interact with the promoters of 83 genes (Supplementary Data 3). Similarly, monocyte Hi-C data²⁷ show 17 SVs overlap potential regulatory regions interacting with promoters of 126 genes. Altogether, non-coding, functional annotations suggest most blood cell trait associated SVs may have an impact on transcriptional regulation.

Fine-mapping and experimental validation of the 9q22.1 (*SIPR3*) monocyte locus

In cases where fine-mapping and functional evidence is similar between trait-associated SVs and correlated SNVs/indels, further experimental follow-up may disentangle the causal variant. To illustrate this point, we performed experimental follow-up on a moderately sized deletion (602 bp) at the 9q22.1 locus. This deletion is near the *SIPR3* gene and was significantly associated with lower monocyte count and lower monocyte percentage (Table 1). This 9q22.1 deletion is also in near perfect LD with a recently reported monocyte-associated SNV (rs28450540) (Fig. 1A, Table 2) and several other SNVs, all of which are relatively specific to individuals of African ancestry (MAF = 0.117).

To characterize the 9q22.1 locus, we compared the overlap between monocyte count-associated variants with deoxyribonuclease I (DNase I) sensitivity, an indicator of accessible chromatin. In several cell types, such as CD34⁺ common myeloid progenitor (CMP) cells and mesenchymal stem cells (MSCs), there was a relative absence of DNase I sensitivity adjacent to or overlying the 9q22.1 locus (Fig. S7A). However, in human primary CD14⁺ monocytes, several peaks of DNase I hypersensitivity overlap the monocyte-associated variants (Fig. 1B). Strikingly, the trait-associated 9q22.1 deletion (9:88923551-88924152) strictly overlapped a DNase I hypersensitivity peak, suggestive of regulatory potential (Fig. 1B). None of the SNVs with $r^2 > 0.8$ with the 9q22.1 deletion directly overlapped DNase I peaks (Fig. 1B). In addition, sequences at the DNase I peak overlapping the 9q22.1 deletion showed

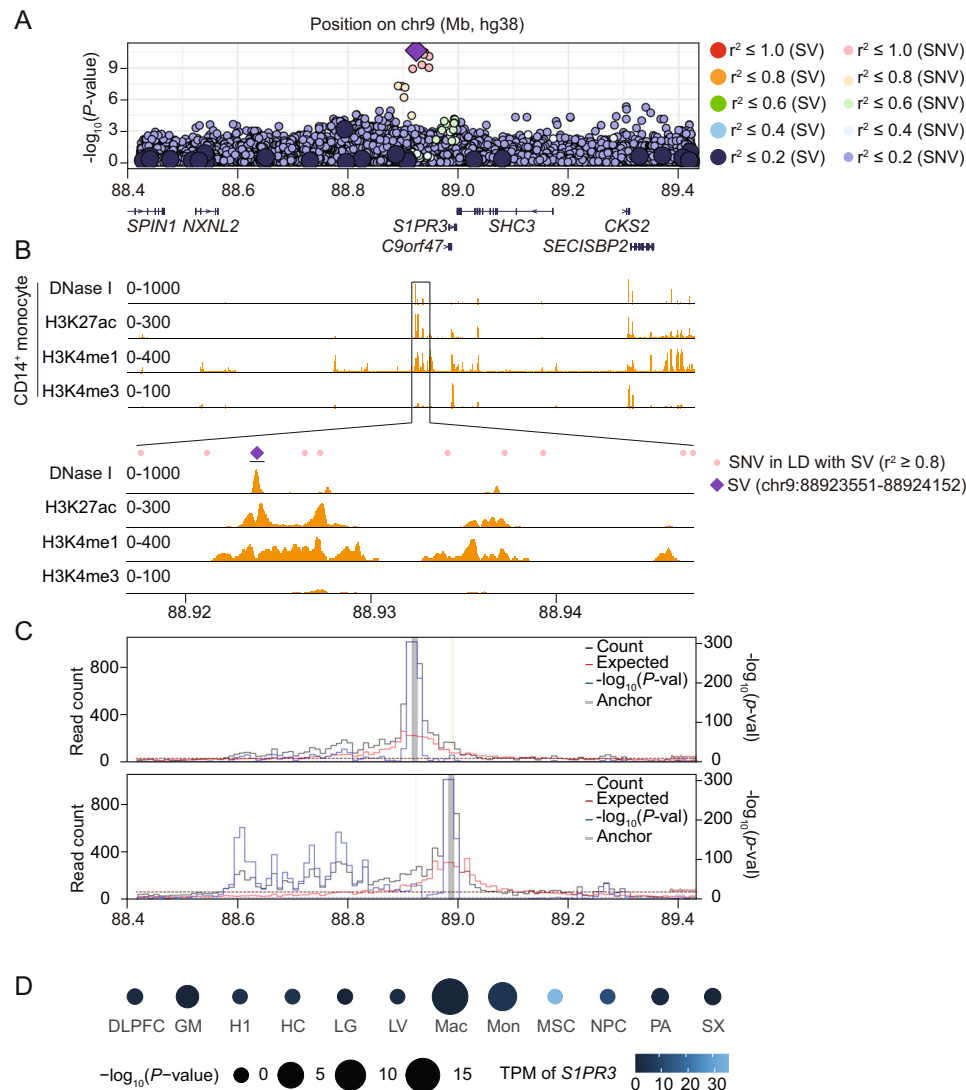


Fig. 1 | A structural variant at human 9q22.1 associated with decreased peripheral monocyte count. All p -values are derived from two-sided t -tests and are not adjusted for multiple comparisons. **A** Genome-wide association $-\log_{10}(p\text{-values})$ for 9q22.1 variants associated with peripheral monocyte counts. The purple diamond represents the trait-associated deletion (9:88923551-88924152); large circles represent other SVs; and small circles represent single nucleotide variants (SNVs) or indels. Color indicates the linkage disequilibrium (LD) calculated in the analysis sample set between the trait-associated deletion and individual SVs and SNVs. **B** Distribution of accessible chromatin (by DNase I sequencing) and histone modifications (H3K27ac, H3K4me1 and H3K4me3) in primary CD14⁺ monocytes across indicated genomic regions from ENCODE²⁶. **C** Virtual 4C plot of long-range chromatin interactions anchored at the trait-associated, 9q22.1 deletion (9:88923551-88924152, upper panel) and the *S1PR3* promoter region (9:91605763-91606263, lower panel), shown as a grey bar, in macrophages. Yellow line highlights the *S1PR3* promoter region (upper panel) trait-associated, 9q22.1 deletion (lower

panel). The observed and expected chromatin contact frequencies (or counts) are represented by the black and red lines, respectively. The left Y axis displays the range of chromatin contact frequency. The statistical significance ($-\log_{10}(P\text{-value})$) of each long-range chromatin interaction is represented by the blue line, with its range listed in the right Y axis. The cell line or tissue specific FDR threshold (5%) is shown as a purple horizontal dashed line, and the more stringent Bonferroni threshold ($P=0.05$) is shown as a maroon horizontal dashed line. **D** Long-range chromatin interaction between the trait-associated, 9q22.1 deletion and *S1PR3* promoter calculated in 12 different cell types. MSC (mesendoderm), NPC (neural progenitor cell), HC (hippocampus), H1 (human embryonic stem cells), LV (left ventricle), PA (pancreas), SX (spleen), DLPCF (dorsolateral prefrontal cortex), LG (lung)³¹, GM (lymphoblast)⁷⁶, Mac (macrophages), Mon (monocytes)²⁷. The circle size represents the magnitude of the $-\log_{10} p$ -value while the color indicates *S1PR3* mRNA level. TPM: transcripts per million.

histone modifications consistent with an enhancer signature in CD14⁺ monocytes, including the presence of H3K27ac and H3K4me1 and absence of H3K4me3 marks (Fig. 1B).

A common feature of distal regulatory elements is long-range interaction with cognate promoters. We investigated these interactions from the viewpoint of the 9q22.1 SV using Hi-C data from monocytes and macrophages²⁷. We observed frequent interactions between the SV-deleted sequences and the *S1PR3* promoter, which is located in the same topologically associating domain (TAD) 67.3 kb downstream (Fig. 1C). Reciprocally, we investigated interactions from

the viewpoint of the *S1PR3* promoter. The interactions between the *S1PR3* promoter and the 9q22.1 SV reached genome-wide significance in macrophage Hi-C data and were just below genome-wide significance in monocyte Hi-C data (Fig. 1C and Fig. S7B). In 10 other Hi-C datasets, including from cell types that express higher levels of *S1PR3* compared to monocytes or macrophages, such as MSCs, we did not observe significant interactions between the *S1PR3* promoter and the 9q22.1 deletion (Fig. 1D). These results suggest the trait-associated 9q22.1 SV overlaps a monocyte/macrophage-specific enhancer element that interacts with *S1PR3*.

Given this regulatory potential, we investigated whether the 9q22.1 SV was associated with expression changes of nearby genes. We performed expression quantitative trait loci (eQTL) analysis on the 9q22.1 SV in the TOPMed Multi-Ethnic Study of Atherosclerosis (MESA, using $n = 169$, including both African American and Hispanic/Latino individuals). *Cis*-eQTL analysis in CD14 + monocyte samples, revealed the strongest association to be between the 9q22.1 SV and *SIPR3* compared to all other genes in a 2 Mb window (Fig. 2A). Deletion of this region is significantly associated with decreased abundance of *SIPR3* ($P = 5.20E-06$) (Fig. 2B). Similar results were observed in peripheral blood mononuclear cells (PBMC), but not in T cells, consistent with a cell type-specific *cis*-regulatory effect on *SIPR3* expression (Figs. S8A, B).

To experimentally test the regulatory potential of the deleted sequences, we performed CRISPRi with dCas9-KRAB in monocytic THP-1 cells. Three sgRNAs were designed targeting different sequences within the 9q22.1 SV deleted segment (Fig. S8C). CRISPRi with each of these three sgRNAs significantly reduced the expression of *SIPR3* but not other nearby genes (Fig. 2C and Fig. S8D–F). Taken together, the results provide strong evidence that the trait-associated SV deletes a monocyte-specific enhancer that controls the expression of *SIPR3* in monocytes.

To test the functional role of *SIPR3* in monocyte maturation and homeostasis, we edited human CD34 + hematopoietic stem and progenitor cells (HSPCs) with three sgRNAs targeting *SIPR3* or a sgRNA targeting a neutral locus and performed *in vitro* monocyte differentiation. Each of the *SIPR3*-targeting sgRNAs yielded highly efficient gene edits ($95.7\% \pm 1.9\%$ indels) (Fig. 2D). Compared with the neutral locus targeting control, each of the three *SIPR3*-edited cell populations showed a significant decrease in CD14 + monocyte differentiation efficiency *in vitro* ($P < 0.001$) (Fig. 2E, F), suggesting monocyte differentiation depends on *SIPR3* expression.

Lastly, to further validate the role of *SIPR3* in human hematopoiesis, we edited human hematopoietic stem and progenitor cells (HSPCs) with sgRNAs targeting a neutral locus or *SIPR3*, and infused the edited HSPCs into immunodeficient NBSGW mice. Human engraftment and multiple-lineage hematopoiesis were analyzed in the mouse bone marrow after 12 weeks. Gene edits were 95.4% in the input HSPC cell product for *SIPR3* and remained consistent (93.7%) in engrafting human cells (Fig. 2G). Overall human hematopoietic chimerism, and the fraction of lymphoid and erythroid lineage cells in the bone marrow was similar between the neutral locus and *SIPR3*-targeting group (Fig. 2H and Fig. S9). We observed a decrease of CD16 + neutrophil percentage ($P = 0.004$) and increase of CD14 + monocyte percentage ($P = 0.02$) in the bone marrow of *SIPR3*-edited groups (Fig. 2I, J). These results suggest that *SIPR3* loss of function leads to altered human myeloid homeostasis *in vivo*, consistent with a functional role of *SIPR3* in determining monocyte count.

Discussion

GWAS have identified thousands of SNVs and small indels that contribute to quantitative hematologic traits but the contribution of SVs to blood cell trait variation has mainly been limited to individuals with rare genetic blood disorders^{32–34}. Here we investigated the contribution of SVs to hematologic variation in ancestrally diverse TOPMed participants. Using single variant tests, we show 21 independent SVs were significantly associated with quantitative hematologic traits. These trait-associated SVs ranged in size (~ 60 bp to >160 kb) and allele frequency. Remarkably, most of these association signals were replicated in independent datasets, suggesting that despite the known challenges associated with SV discovery/genotyping in short-read data⁶, WGS-based SV call-sets can be successfully used to study complex trait variation.

Most trait-associated SVs are located in genomic regions previously associated with blood cell traits and most are not conditionally

independent of SNV/indels at the same loci previously identified through GWAS. One exception was a novel association between the 17p11.2 locus (*KCNJ18* SV) and white blood cell-related phenotypes. *KCNJ18* has no known role in leukocyte biology. It encodes a potassium channel and variants in this gene are associated with the Mendelian disorder, thyrotoxic hypokalemic periodic paralysis [MIM:613239]. Moreover, the trait-associated *KCNJ18* SV is located in a complex region of the genome which includes a segmental duplication near the centromere of chromosome 17. Likely due to this complexity, we did not identify a *KCNJ18* SV representative in replication datasets. Based on these results as well as the associated phenotypic pattern (opposing effects on neutrophil and lymphocyte proportions) additional analyses are required to ensure this finding reflects inherited genetic variation.

Functional annotation indicates most trait-associated SVs are located in non-coding regions of the genome. The majority of trait-associated SVs were predicted to impact regulatory elements or chromatin loop structure and chromatin domain boundaries. Together with LD and conditional analyses, this is consistent with the notion that SVs may provide mechanistic insights for a subset of known GWAS loci. For instance, a chr7 deletion which includes the EPO promoter was recently shown to alter iPSC expression levels of 5 nearby genes³⁵, including the genes, *TFR2* and *EPHB4* which are involved in iron metabolism and erythropoiesis^{36,37}. In our analyses, this chr7 deletion was present in TOPMed (allele frequency = 0.189) but just missed our significance threshold for association with red cell phenotypes. Notably, in our analyses this chr7 deletion was in near perfect LD with a previously-reported SNV chr7:100729121 (rs4729607)⁹.

In this study, we also identified a monocyte trait-associated SV (602 bp, 9q22.1 deletion) that directly overlaps a monocyte cell type-specific enhancer with accessible chromatin and enhancer signature histone modifications. The enhancer forms a physical interaction with the *SIPR3* gene in monocytes, and the 9q22.1 SV is an eQTL for *SIPR3* expression in monocytes. By using CRISPRi targeting the enhancer, we showed the enhancer positively regulates *SIPR3* in monocyte lineage cells. Prior GWAS have identified SNVs at this locus associated with blood cell traits including monocyte count, but without identification of the causal variant. This trait association represents an experimentally validated example where an ancestry-specific SV appears to underlie an SNV-tagged trait association through effects on cell-type specific gene regulation.

Gene editing of *SIPR3* significantly impacted both *in vitro* monocyte maturation and monocyte homeostasis in xenograft experiments. *SIPR3*, a receptor for the bioactive lipid sphingosine-1-phosphate (S1P), is a central regulator which drives myeloid differentiation³⁸. Complementary to our results, previous studies have shown that *SIPR3* overexpression alone is sufficient to induce myeloid differentiation in human HSC³⁸. In addition, *SIPR3* has been implicated in the mobilization from the bone marrow to the peripheral blood of hematopoietic and mesenchymal progenitors^{39,40}. The decreased efficiency of *in vitro* monocyte maturation, and relative increase in the fraction of bone marrow CD14⁺ monocytes with reciprocal decrease of bone marrow CD16⁺ neutrophils of engrafted mice, may suggest that *SIPR3* both plays cell autonomous roles in monocytes during maturation as well as impacts the trafficking of myeloid cells from bone marrow stores to circulating cells in the peripheral blood. Supporting this hypothesis, S1P receptors, which are chemotactically sensitive to S1P gradients, regulate multiple processes, including migration, matrix adhesion, and cell-cell contact. Therefore, the steep gradient of S1P concentration existing between bone marrow and blood might promote monocytes to navigate from the bone marrow to circulation⁴⁰. The biological contributions of *SIPR3* to monocyte maturation and trafficking may be complex and could merit future dedicated study.

In summary, our results from a large ancestrally-diverse population-based data set add further evidence that complex trait association

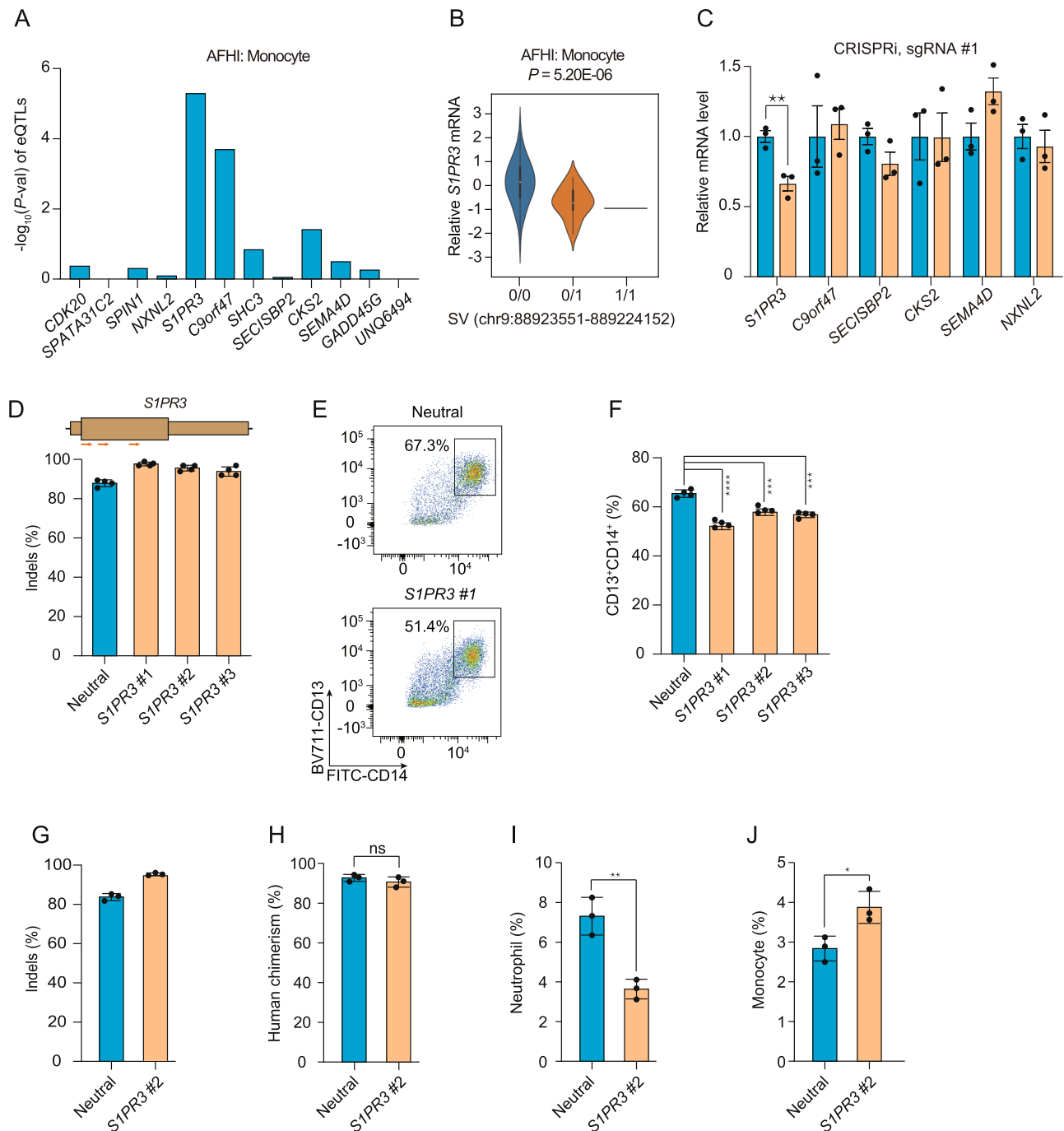


Fig. 2 | Genome and epigenome editing implicates *SIPR3* in the 9q22.1 monocyte association. All p -values are derived from two-sided t -tests (unless otherwise indicated) and are not adjusted for multiple comparisons. **A** eQTL results between the 9q22.1 SV and genes within 1-Mb window in monocytes using data from MESA, including $n = 77$ AA and $n = 92$ Hispanic/Latino participants. AFHI: African American and Hispanic/Latino. **B** Violin plot (with minima, maxima, median, and inter-quartile range) demonstrating the correlation between the 9q22.1 SV genotype and expression of *SIPR3*, in $n = 169$ from MESA. **C** Expression of genes within a 2 Mb window in THP-1 cells expressing dCas9-KRAB after transduction with an sgRNAs targeting the SV (orange) as compared to a neutral locus control sgRNA (blue). Relative mRNA level of each gene was represented by mean \pm standard deviation (SD). $N = 3$ biological replicates, where each replicate is a unique cellular transduction by sgRNA cassette. $**P = 0.009$. Location of sgRNAs designed for CRISPRi are indicated in Fig. S8C. **D–F** *SIPR3* gene editing impaired monocyte differentiation in vitro. **D** Editing efficiency in HSPCs following 3xNLS-SpCas9:sgRNA electroporation with the indicated sgRNA. Gene edits were

measured after 4 days of electroporation ($N = 4$ biological replicates). Location of *SIPR3* coding sequence targeting sgRNAs are indicated above. **E** Representative flow cytometry indicating CD13 $^+$ CD14 $^+$ cell populations from the neutral locus and *SIPR3* targeting group after 12-day differentiation. **F** CD13 $^+$ CD14 $^+$ percentage in the *SIPR3* targeting group and the neutral locus targeting group. $N = 4$ replicates where each replicate is a unique Cas9:sgRNA electroporation experiment. Mean \pm SD, with Student's two-sided t -test. $***P < 0.001$, $****P < 0.0001$. **G–J** Human CD34 $^+$ HSPCs from three healthy donors were edited by Cas9 RNP electroporation (EP) targeting a neutral locus and *SIPR3* coding sequence infused into NBSGW mice 24 h after electroporation. After 12 weeks, engrafted bone marrow was characterized by immunophenotyping. **G** Indels determined by Sanger sequencing before transplantation. (H–J) Quantification of different human cell types between the neutral locus and *SIPR3* targeting group. Human chimerism, hCD45 $^+$; Monocytes, hCD45 $^+$ CD33 $^+$ SScLowCD14 $^+$; neutrophil, hCD45 $^+$ CD33 $^+$ SScHighCD16 $^+$. $N = 3$ independent biological replicates, each replicate indicates one mouse. Mean \pm SD, 2-sided Mann-Whitney test. $*P = 0.025$, $**P = 0.004$.

signals may be explained by the presence of structural variation. These findings complement recent WGS-based studies performed in European population isolates demonstrating the contribution of structural variation to complex trait variation (quantitative cardiometabolic and anthropometric traits)^{5,17}. Several limitations of our study should be noted: 1) our analyses were restricted to deletions, inversions, and duplication and 2) were restricted to autosomal structural variation. Both of these limitations can be overcome with additional SV association studies that more broadly survey structural variation. In particular, the incorporation of long-read data into SV-based association analyses will greatly improve our understanding of how SVs contribute to hematological and complex trait variation.

Methods

TOPMed study population

We included 50,675 participants from 12 TOPMed studies: Genetics of Cardiometabolic Health in the Amish (Amish, $n = 1090$)⁴¹, Atherosclerosis Risk in Communities Study (ARIC, $n = 3717$)⁴², Mount Sinai BioMe Biobank (BioMe, $n = 9102$)⁴³, Coronary Artery Risk Development in Young Adults (CARDIA, $n = 2966$)⁴⁴, Cardiovascular Health Study (CHS, $n = 3478$)⁴⁵, Genetic Epidemiology of COPD Study (COPDGene, $n = 5595$)⁴⁶, Framingham Heart Study (FHS, $n = 2760$)⁴⁷, Genetic Studies of Atherosclerosis Risk (GeneSTAR, $n = 1494$)⁴⁸, Hispanic Community Health Study - Study of Latinos (HCHS_SOL, $n = 3824$)⁴⁹, Jackson Heart Study (JHS, $n = 3329$)^{50,51}, Multi-Ethnic Study of Atherosclerosis (MESA, $n = 2516$)⁵², and Women's Health Initiative (WHI, $n = 10,804$)⁵³. The 50,675 TOPMed participants were categorized into discrete ancestry subgroups using a machine learning algorithm, which uses genetically inferred ancestry to refine self-identified ancestry and impute missing values⁵⁴ (see Supplemental Methods). The ancestry composition in this study was 59% European, 24% African, 16% Hispanic/Latino, and 1% Asian (Supplementary Data 1). Only samples with a missingness rate <10% in the structural variant dataset were included in analysis. Further descriptions of the design of the participating TOPMed cohorts and the sampling of individuals within each cohort for TOPMed WGS are provided in the section "Participating TOPMed studies" under Supplemental Methods. All studies were approved by the appropriate institutional review boards (IRBs) and informed consent was obtained from all participants.

Blood cell trait measurements

Red blood cell, white blood cell and platelet quantitative traits were measured from freshly collected whole blood samples using automated hematology analyzers according to clinical laboratory standards. In studies where multiple blood cell measurements per participant were available, we selected a single measurement for each trait and each participant. Each trait was defined as follows: Hematocrit (HCT) is the percentage of volume of blood that is composed of red blood cells. Hemoglobin (HGB) is the mass per volume (grams per deciliter) of hemoglobin in the blood. Mean corpuscular hemoglobin (MCH) is the average mass in picograms of hemoglobin per red blood cell. Mean corpuscular hemoglobin concentration (MCHC) is the average mass concentration (grams per deciliter) of hemoglobin per red blood cell. Mean corpuscular volume (MCV) is the average volume of red blood cells, measured in femtoliters (fL). RBC count is the count of red blood cells in the blood, by number concentration in millions per microliter. Red cell distribution width (RDW) is the measurement of the ratio of variation in width to the mean width of the red blood cell volume distribution curve taken at \pm one CV. Total white blood cell count (WBC), neutrophil, monocyte, lymphocyte, eosinophil, basophil and platelet count are defined with respect to cell concentration in blood, measured in thousands/microliter. The proportion of neutrophils, monocytes, lymphocytes, or eosinophils were calculated by dividing the respective WBC sub-type count by the total measured WBC. Mean platelet volume (MPV) was measured in fL. For each trait,

we identified extreme values that may represent measurement or recording errors or hematologic malignancies and removed them from the analysis.

In a subset of samples from the JHS and HCHS/SOL studies, we evaluated four iron-related phenotypes: serum iron, total iron binding capacity (TIBC), transferrin saturation, and ferritin. Serum iron ($\mu\text{g}/\text{dl}$) was measured by colorimetric assay using a ferrozine reagent (Roche Diagnostics, Indianapolis, IN). Unsaturated iron binding capacity (UIBC) was assayed by colorimetric assay on the same sample, TIBC ($\mu\text{g}/\text{dl}$) was calculated by the formula: $\text{TIBC} = \text{serum iron} + \text{UIBC}$. Serum ferritin (ng/ml) was measured with Roche reagents using a particle enhanced immunoturbidimetric assay. Transferrin saturation (%) was calculated by the formula: $\text{SAT} = \text{serum iron}/\text{TIBC} \times 100$.

WGS data and quality control in TOPMed

WGS was performed through the NHLBI TOPMed program on genomic DNA isolated from peripheral blood. WGS was generated to an average depth of 38X by six sequencing centers (Broad Genomics, Northwest Genomics Center, Illumina, New York Genome Center, Baylor, and McDonnell Genome Institute)⁵⁵. Most WGS was performed using PCR-free library preparation, Illumina HiSeq X Ten or NovaSeq instruments and 150 bp paired end reads. Sequencing reads were aligned to the human reference genome (GRCh38) by the TOPMed Informatics Research Center (IRC) using the read mapping pipeline described in Regier, A. et al.⁵⁶.

Single nucleotide variant and small indel discovery and genotyping in TOPMed

We utilized the TOPMed freeze 8 genotype call set produced by the IRC as previously described⁵⁶. Briefly, SNVs and indels were discovered on a per sample basis, then merged and genotyped across samples. SNV and indel quality control (QC), was performed by calculating Mendelian consistency scores and by applying a support vector machine (SVM) classifier trained on known variant sites and Mendelian inconsistencies. SNV- and indel-based, sample QC measures included: concordance between annotated and inferred genetic sex, concordance between prior array genotype data and TOPMed WGS data, and pedigree checks. Further details regarding data processing, and quality control are described on the TOPMed website (<https://www.nhlbiwgs.org/topmed-whole-genome-sequencing-methods-freeze-8>) and in a common document accompanying each TOPMed study's dbGaP accession.

Structural variant discovery and genotyping in TOPMed

We utilized the TOPMed SV freeze 1.0 call set, which contains 138,134 TOPMed samples. Briefly, SV calls were assessed from each sample separately using Parliament2 pipeline¹⁵. The Parliament2 pipeline provides the union of SV calls from six different programs: BreakDancer, BreakSeq, CNVnator, Delly, Lumpy and Manta. SV calls were merged across samples using survivor⁵⁷ and filtered using SVTyper⁵⁸. Sample genotypes for each variant were assessed using muCNV¹⁶. After final filtering, the TOPMed SV freeze 1.0 call set consists of a total of 466,455 autosomal SV sites: 231,817 deletions, 197,412 duplications and 37,226 inversions. Of these, 96,049 had $\text{MAC} \geq 5$ in at least one trait and were included in association analyses. For association analysis, the genotypes of each SV were represented in a bi-allelic genotype format ($\text{GT} = 0/0, 0/1, 1/1$), similar to SNVs and small indels generated from the same WGS data.

Single variant association analysis of SVs and blood cell traits using linear mixed models

Single variant SV association tests for all variants with a minor allele count (MAC) ≥ 5 were performed for each blood cell trait using a two-stage linear mixed model (LMM) approach implemented in the GENESIS software^{59,60}. In the first stage, a null model assuming no

association between the outcome and any SV was fit, adjusting for the fixed effect covariates of: age at trait measurement; sex; a variable indicating TOPMed study and study phase (study_phase); indicators for stroke, COPD, and VTE; the first 11 PC-AiR⁶¹ principal components (PCs) of genetic ancestry as estimated from the WGS SNV/indel genotypes. We additionally included as fixed effect covariates, the first 10 principal components estimated from read depth (“batch PCs”). To calculate batch PCs, we first computed the average sequencing depth for every 1 kb genomic region (“bin”) across the 22 autosomes⁶². We removed bins containing repetitive sequences with poor mappability (<1.0 using 50 bp k-mers in GEMTools v1.759) or sequences overlapping known CNVs in the Database of Genomic Variants. Following normalization of the approximately 150,000 remaining bins, we performed Randomized Singular Value Decomposition (rSVD)⁶³, to generate batch PCs, which were used to correct for batch and technical artifacts arising from the sequencing process.

In the first-stage null model, a 4th degree sparse empirical kinship matrix (KM) computed with PC-Relate⁶⁴ was included to account for genetic relatedness among participants. To control genomic inflation, we additionally allowed for heterogeneous residual variances by study and ancestry group. Details on how ancestry groups were estimated for this adjustment are in the supplemental methods. Following fitting of the first-stage null model, we performed a rank-based inverse-normal transformation of the marginal residuals, and subsequently rescaled the residuals by their variance prior to transformation. This rescaling allows for clearer interpretation of estimated SV genotypic effect sizes from the subsequent association tests. In the second stage, we fit another LMM using the rank-normalized and rescaled residuals as the outcome, with the same fixed effect covariates, sparse KM, and heterogeneous residual variance model as in Stage 1. The output of the Stage 2 null model was then used to perform genome-wide score tests of genetic association for all SVs that passed the TOPMed SV quality filters and with a minor allele count (MAC) ≥ 5 . Missing SV genotype calls were imputed to the mean before performing the association tests. Investigation of QQ plots stratified by MAC showed similar test behavior at all MAC bins (Fig. S2). The total number of unique SVs tested across all traits was 96,049.

Basophils was tested as a binary outcome (basophil count > 0), so the null model was fit as a logistic mixed model using the GMMAT method as implemented in GENESIS, rather than a two-stage LMM. The same fixed effect covariates and sparse KM were used in the null model, and score tests were used for association. Genome-wide significance was defined as 5.0×10^{-8} for common variants (MAF > 1%) and 8.0×10^{-9} for rare variants (MAF < 1%)⁶⁵.

Visualization of SVs associated with blood cell traits

For SVs significantly associated with blood cell traits, we performed additional quality control by visualizing aligned WGS reads in variant samples. Visualization was performed using samplot on the NHLBI Biodata Catalyst cloud computing platform (<https://doi.org/10.5281/zenodo.3822858>). For each SV event, we visualized aligned reads for multiple samples and excluded any SV events that were not clearly supported by the aligned WGS data. Additionally, we selected SV events in instances where Parliament2 identified multiple overlapping SVs by different SV calling algorithms. This was concluded following data visualization and we selected SVs based on the resolution of predicted Parliament2 breakpoints.

Replication of trait-associated SVs using deCODE genetics and UK Biobank datasets

We performed replication analyses for each TOPMed SV-blood cell trait association signal using deCODE genetics and UKBB datasets. Briefly, SVs were called in Icelanders (deCODE genetics) using 49,962 short-read^{18,19} and 3622 long-read sequenced¹⁷ individuals. These data

were phased and all genotyped variants were imputed into 166,281 individuals using a previously described methodology^{66,67}. SVs were called from 150,119 short-read sequenced individuals in UKBB. Three cohorts were used in UKBB with 132,169, 2963, and 3047 sequenced and 431,805, 9633, and 9252 imputed individuals, in British/Irish (XBI), African (XAF) and South Asian (XSA) populations, respectively²⁰. For replication analyses, we defined an SV in replication datasets to represent a TOPMed SV, if located within 5 kb of the TOPMed SV and if the two SV sizes overlapped by at least 25%. We considered SVs as representative if they were the same structural variant type (e.g. both SVs were deletions) and had similar minor allele frequencies in the relevant population. We tested for association for all representative SVs and their corresponding phenotypes based on the linear mixed model implemented in BOLT-LMM⁶⁸ and described in^{17,20}. We considered an association to be replicated if at least one of the *p*-values from the deCODE, UKBB British, UKBB African, or UKBB South Asian cohorts was < 0.05/(number of its representative SVs in given dataset).

Functional annotation of SVs

We annotated genome sequence information for SVs significantly associated with blood cell traits using AnnoSV⁶⁹. From AnnoSV, we ascertained gene annotations (based on RefSeq, ENSEMBL), the presence of similar SVs in genomic databases (e.g., DGV) and breakpoint information including overlap with repetitive elements. To understand the potential impact of trait-associated SVs on non-coding/regulatory regions, we cross-referenced SVs with five different genomic annotations including, frequently interacting regions (FIREs) from Hi-C data^{30,31}, topologically associating domain (TAD) boundaries, cell-type specific regulatory networks from super interactive promoters (SIPs)²⁹, candidate *cis* regulatory elements (cCREs) from ENCODE, and chromatin interaction information from chromatin conformation data including Hi-C²⁷ and promoter capture Hi-C (pChi-C)²⁸.

Linkage disequilibrium and conditional analyses for trait-associated SVs

For each blood cell trait, we performed conditional association analyses to determine which genome-wide significant SVs remained significant following adjustment for (1) previously reported GWAS variants and (2) SNV and small indels previously detected in TOPMed^{21–23}. To address the first question, we used variants detected in multi-ancestry and European populations reported in Chen et al. 2020 and Vuckovic et al. 2020^{9,10}. The genome-wide significant variants from Chen et al. 2020 and Vuckovic et al. 2020 were matched to TOPMed SNVs and small indels that passed the IRC quality filters based on chromosome, position, and alleles. For each trait, the set of matched variants on each chromosome was then LD-pruned at $r^2 = 0.8$ in the sample set of the non-conditional analysis for that trait, preferentially keeping variants with lower *p*-values in the TOPMed analysis sample set. Switching the LD threshold to $r^2 = 0.999$ for pruning produced very similar *p*-values and did not add or remove any significant loci. This pruned set of variants were combined across chromosomes and included as fixed effect covariates in the null model using the same fully-adjusted two-stage LMM association testing procedure described above^{59,60}. To identify SVs independent of GWAS variants detected in the TOPMed data, we used a similar procedure, starting with any SNV or small indels with $P < 5.0 \times 10^{-8}$ in single variant association tests using the same sample set for the trait. This set of variants was then LD-pruned at $r^2 = 0.8$, again preferentially keeping variants with lower *p*-values, and included as fixed effects in a two-stage LMM association testing^{59,60}.

To investigate the proportion of SVs in LD with known, blood-cell trait SNVs/indels, we additionally calculated LD (r^2) for genotypes of 6652 previously-reported SNVs/indels from European ancestry samples¹⁰ and SVs with MAC ≥ 5 on the same chromosome. Only

TOPMed participants with inferred European ancestry ($N = 29,244$) were used for the LD calculation. Each SNV/indel was then matched to the SV with the highest r^2 value.

eQTL analysis

RNA-sequencing (RNA-seq) data for eQTL analysis were derived from a subsample of African American and Hispanic/Latino TOPMed MESA cohort participants using blood samples derived from either MESA exam 1 (2000-2002) or MESA exam 5 (2010-2012) as previously described⁷⁰. RNA sequencing was performed on peripheral blood mononuclear cells (PBMC) from 297 African American and 246 Hispanic/Latino MESA participants at exam 1 and from isolated monocytes and T lymphocytes from 77 African American and 92 Hispanic/Latino MESA participants at exam 5 RNA-seq data was processed following the TOPMed harmonized RNA-seq pipeline. Specifically, gene-level expression was quantified by RSEM v1.3.0. We performed cis-eQTL analysis (± 1 Mb) to identify genes whose expression is associated with 9q22.1 SV using Matrix eQTL⁷¹.

Hematopoietic cell lines

THP-1 cells (Cat# TIB-202) were obtained from the American Type Culture Collection and cultured in RPMI 1640 (Thermo Fisher Scientific, USA). To make the complete growth medium, the following components were added: 2-mercaptoethanol (Cat# 21985-023, Thermo Fisher Scientific) to a final concentration of 0.05 mM; fetal bovine serum (Cytiva) to a final concentration of 10%.

Primary hematopoietic cells and monocyte-macrophage differentiation

Human CD34⁺ HSPCs from mobilized peripheral blood of deidentified healthy donors were purchased from Fred Hutchinson Cancer Research Center, Seattle, Washington. CD34⁺ HSPCs were cultured in StemSpan SFEM medium (Cat# 09650, STEMCELL Technologies) supplemented with 1x StemSpan CD34⁺ expansion supplement (Cat# 02691, STEMCELL Technology). To induce monocyte-macrophage differentiation from CD34⁺ HSPCs, the cytokine cocktail of M-CSF 30 ng/mL, FLT3-Ligand 100 ng/mL, SCF 50 ng/mL, IL-3 5 ng/mL, IL-6 3 ng/mL and L-Glutamine 2 mM was supplemented to the culture media for 11 days before analysis. GM-CSF 5 ng/mL was supplemented in the culture media for the first 4 days. All cytokines of human origin and from PeproTech.

CRISPR/Cas9 guide design, cloning, lentiviral vector production and transduction and 3xNLS-SpCas9 preparation

Streptococcus pyogenes Cas9 (SpCas9) guide RNAs that either target *SIPR3* coding sequence or bind near the structural deletion (9:88923551-8892452) were identified using computational algorithms with prioritization for on-target efficiency and reduced off-target effects (CRISPOR: <http://crispor.tefor.net/>). For RNP experiments, the chemically modified sgRNAs were synthesized by Integrated DNA Technologies. SpCas9 proteins were expressed and purified as previously described⁷².

For CRISPRi experiments, oligos (from GENEWIZ company) were annealed and ligated into LentiGuide-Puro (Addgene, Cat#52963). Following lentiviral production and transduction into THP-1 cell lines with stable dCas9-KRAB expression (Addgene, Cat#89567), 10 μ g/ml blasticidin and 1 μ g/ml puromycin were added to select for sgRNA expression in cells with stable dCas9-KRAB expression. The sequence of sgRNAs are summarized in Supplementary Data 4.

CRISPR-Cas9 genome editing in CD34⁺ HSPCs and THP-1 cells

CD34⁺ HSPCs and THP-1 cells were maintained in their favorable medium (see before) 24 h before electroporation. Approximately 100,000 cells per condition were electroporated using the Lonza 4D nucleofector with 100 pmol 3xNLS-SpCas9 protein and 300 pmol

modified sgRNA targeting the locus of interest. In addition to mock treated cells, “safe-targeting” RNPs were used as experimental controls as indicated in each figure legend⁷³. After electroporation, cells were induced for monocyte-macrophage differentiation as described previously. Genomic DNA was isolated from an aliquot of cells, the sgRNA targeted locus was amplified by PCR which was subject to Sanger sequencing and then TIDE analysis to quantify indel spectrum at day 4 after electroporation.

Determination of target gene expression

Total RNA was extracted from cell cultures 4 days after electroporation using the RNeasy Plus Mini Kit (QIAGEN) and reverse transcribed using the iScript cDNA synthesis kit (Biorad) according to the manufacturer’s instructions. Expression of target genes was quantified using real-time RT-qPCR with GAPDH as an internal control. All gene expression data represent the mean of at least three biological replicates. Primers for PCR are summarized in Supplementary Data 5. Since PCR primers could not be designed for RP5-1050E16.1, this gene was excluded from further analysis.

Flow cytometry analysis

For analysis of surface markers, cells were stained in PBS containing 2% (w/v) BSA, with the following antibodies (from BioLegend): anti-human CD34 (clone 581, Cat# 343504, 1:200), anti-human CD33 (clone P67.6, Cat# 366608, 1:200), anti-human CD117 (clone 104D2, Cat# 313205, 1:200), anti-human CD16 (clone 3G8, Cat# 302046, 1:100), anti-human CD14 (clone 63D3, Cat# 367117, 1:200). Monocyte and macrophage were indicated by anti-human CD14⁺. Flow cytometry data were acquired on a LSRII or LSR Fortessa (BD Biosciences) and analyzed using FlowJo software (Tree Star).

Immunophenotyping of human CD34⁺ HSPCs xenograft from NBSGW mice

NOD.Cg-KitW-4J Tyr^b Prkdcscid Il2rgtm1Wjl (NBSGW) mice were obtained from Jackson Laboratory (Stock 026622) and kept in 12 h of light at room temperature. CD34⁺ HSPCs were maintained and edited as described above. Cells were allowed to recover for 24 h after electroporation, and then infused by retro-orbital injection into non-irradiated NBSGW female mice. Bone marrow was isolated for human xenograft analysis 16 weeks after human CD34⁺ HSPCs engraftment. For flow cytometry analysis, bone marrow cells were first incubated with Human TruStain FcX (BioLegend, Cat# 422302) and TruStainFcX (anti-mouse CD16/32, 101320, BioLegend) blocking antibodies for 10 min and then stained with marker panels designed for multi-lineage analysis. The following antibodies were used: From BD: anti-mouse CD45 (clone 30-F11, Cat# 561487, 1:100), anti-human CD45 (clone HI30, Cat# 560367, 1:200) From BioLegend: anti-human CD34 (clone 581, Cat# 343504, 1:200), anti-human CD33 (clone P67.6, Cat# 366608, 1:200), anti-human CD117 (clone 104D2, Cat# 313205, 1:200), anti-human CD16 (clone 3G8, Cat# 302046, 1:100), anti-human CD14 (clone 63D3, Cat# 367117, 1:200), anti-human CD235a (clone HI264, Cat# 349104, 1:100), anti-human CD3 (clone UCHT1, Cat# 300412, 1:200), anti-human CD19 (clone HIB19, Cat# 302212, 1:200), and Fixable Viability Dye eFluor 780 for live/dead staining (65-0865-14, Thermo Fisher, 1:10000). Percentage human engraftment was calculated as hCD45⁺ cells/(hCD45⁺ + mCD45⁺ cells). The mouse work was performed, following Boston Children’s Hospital institutional review board (IRB) approval.

DNase I-sequencing, chromatin, and Hi-C datasets

DNase I-sequencing and histone modification datasets, including H3K27ac, H3K4me1 and H3K4me3, were downloaded from the ENCODE project²⁶, and were then analyzed using WashU Epigenome Browser online software⁷⁴. In situ Hi-C maps of DNA interactions in human monocytes and macrophages were previously described²⁷, and

visualized by HUGIn2 (Hi-C Unifying Genomic Interrogator, <http://hugin2.genetics.unc.edu/Project/hugin/>)⁷⁵.

Reporting summary

Further information on research design is available in the Nature Portfolio Reporting Summary linked to this article.

Data availability

Data for each participating study can be accessed through dbGaP with the corresponding accession numbers (Amish, phs000956; ARIC, phs001211; BioMe, phs001644; CARDIA, phs001612; CHS, phs001368; COPDGene, phs000951; FHS, phs000974; GeneSTAR, phs001218; HCHS/SOL, phs001395; JHS, phs000964; MESA, phs001416; WHI, phs001237).

Code availability

Code to implement the associations analyses is available on GitHub at https://github.com/UW-GAC/analysis_pipeline.

References

- Weischenfeldt, J., Symmons, O., Spitz, F. & Korb, J. O. Phenotypic impact of genomic structural variation: Insights from and for human disease. *Nat. Rev. Genet.* **14**, 125–138 (2013).
- Stankiewicz, P. & Lupski, J. R. Structural variation in the human genome and its role in disease. *Annu. Rev. Med.* **61**, 437–455 (2010).
- Aguirre, M., Rivas, M. A. & Priest, J. Phenome-wide burden of copy-number variation in the UK biobank. *Am. J. Hum. Genet.* **105**, 373–383 (2019).
- Boettger, L. M. et al. Recurring exon deletions in the HP (haptoglobin) gene contribute to lower blood cholesterol levels. *Nat. Genet.* **48**, 359–366 (2016).
- Chen, L. et al. Association of structural variation with cardiometabolic traits in finns. *Am. J. Hum. Genet.* **108**, 583–596 (2021).
- Sudmant, P. H. et al. An integrated map of structural variation in 2,504 human genomes. *Nature* **526**, 75–81 (2015).
- Chiang, C. et al. The impact of structural variation on human gene expression. *Nat. Genet.* **49**, 692–699 (2017).
- Astle, W. J. et al. The allelic landscape of human blood cell trait variation and links to common complex disease. *Cell* **167**, 1415–1429.e19 (2016).
- Chen, M.-H. et al. Trans-ethnic and ancestry-specific blood-cell genetics in 746,667 individuals from 5 global populations. *Cell* **182**, 1198–1213.e14 (2020).
- Vuckovic, D. et al. The polygenic and monogenic basis of blood traits and diseases. *Cell* **182**, 1214–1231.e11 (2020).
- Harteveld, C. L. & Higgs, D. R. α -thalassaemia. *Orphanet J. Rare Dis.* **5**, 1–21 (2010).
- Chen, Z. et al. Genome-wide association analysis of red blood cell traits in African Americans: The COGENT Network. *Hum. Mol. Genet.* **22**, 2529–2538 (2013).
- Raffield, L. M. et al. Common α -globin variants modify hematologic and other clinical phenotypes in sickle cell trait and disease. *PLoS Genet.* **14**, e1007293 (2018).
- Paterson, A. D. et al. Persons with Quebec platelet disorder have a tandem duplication of PLAU, the urokinase plasminogen activator gene. *Blood* **115**, 1264–1266 (2010).
- Zarate, S. et al. Parliament2: Accurate structural variant calling at scale. *Gigascience* **9**, 1–9 (2020).
- Jun, G. et al. muCNV: Genotyping structural variants for population-level sequencing. *Bioinformatics* **37**, 2055–2057 (2021).
- Beyter, D. et al. Long-read sequencing of 3,622 Icelanders provides insight into the role of structural variants in human diseases and other traits. *Nat. Genet.* **53**, 779–786 (2021).
- Eggertsson, H. P. et al. GraphTyper2 enables population-scale genotyping of structural variation using pangenome graphs. *Nat. Commun.* **10**, 5402 (2019).
- Niehus, S. et al. PopDel identifies medium-size deletions simultaneously in tens of thousands of genomes. *Nat. Commun.* **12**, 730 (2021).
- Halldorsson, B. V. et al. The sequences of 150,119 genomes in the UK biobank. *bioRxiv* 2021.11.16.468246 <https://doi.org/10.1101/2021.11.16.468246> (2021).
- Hu, Y. et al. Whole-genome sequencing association analysis of quantitative red blood cell phenotypes: The NHLBI TOPMed program. *Am. J. Hum. Genet.* **108**, 1165 (2021).
- Mikhaylova, A. V. et al. Whole-genome sequencing in diverse subjects identifies genetic correlates of leukocyte traits: The NHLBI TOPMed program. *Am. J. Hum. Genet.* **108**, 1836–1851 (2021).
- Little, A. et al. Whole genome sequence analysis of platelet traits in the NHLBI trans-omics for precision medicine initiative. *Hum. Mol. Genet.* <https://doi.org/10.1093/hmg/ddab252> (2021).
- Kammers, K. et al. Transcriptional profile of platelets and iPSC-derived megakaryocytes from whole-genome and RNA sequencing. *Blood* **137**, 959–968 (2021).
- Chi, X., Li, Y. & Qiu, X. V(D)J recombination, somatic hypermutation and class switch recombination of immunoglobulins: mechanism and regulation. *Immunology* **160**, 233–247 (2020).
- ENCODE Project Consortium. The ENCODE (Encyclopedia Of DNA Elements) Project. *Science* **306**, 636–640 (2004).
- Phanstiel, D. H. et al. Static and Dynamic DNA Loops form AP-1-bound activation hubs during macrophage development. *Mol. Cell* **67**, 1037–1048.e6 (2017).
- Javierre, B. M. et al. Lineage-specific genome architecture links enhancers and non-coding disease variants to target gene promoters. *Cell* **167**, 1369–1384.e19 (2016).
- Lagler, T. M. et al. Super interactive promoters provide insight into cell type-specific regulatory networks in blood lineage cell types. *bioRxiv* 2021.03.15.435494 <https://doi.org/10.1101/2021.03.15.435494> (2021).
- Crowley, C. et al. FIREcaller: Detecting frequently interacting regions from Hi-C data. *Comput. Struct. Biotechnol. J.* **19**, 355–362 (2021).
- Schmitt, A. D. et al. A compendium of chromatin contact maps reveals spatially active regions in the human genome. *Cell Rep.* **17**, 2042–2059 (2016).
- Liang, M. et al. Enhancer-gene rewiring in the pathogenesis of Quebec platelet disorder. *Blood* **136**, 2679–2690 (2020).
- Giannuzzi, G. et al. The Human-Specific BOLA2 Duplication Modifies Iron Homeostasis and Anemia Predisposition in Chromosome 16p11.2 Autism Individuals. *Am. J. Hum. Genet.* **105**, 947–958 (2019).
- Turro, E. et al. Whole-genome sequencing of patients with rare diseases in a national health system. *Nature* **583**, 96–102 (2020).
- Jakubosky, D. et al. Properties of structural variants and short tandem repeats associated with gene expression and complex traits. *Nat. Commun.* **11**, 2927 (2020).
- Suenobu, S. et al. A role of EphB4 receptor and its ligand, ephrin-B2, in erythropoiesis. *Biochem. Biophys. Res. Commun.* **293**, 1124–1131 (2002).
- Richard, C. & Verdier, F. Transferrin Receptors in Erythropoiesis. *Int. J. Mol. Sci.* **21**, 9713–9729 (2020).
- Xie, S. Z. et al. Sphingosine-1-phosphate receptor 3 potentiates inflammatory programs in normal and leukemia stem cells to promote differentiation. *Blood Cancer Disco.* **2**, 32–53 (2021).
- Ogle, M. E. et al. Sphingosine-1-Phosphate Receptor-3 supports hematopoietic stem and progenitor cell residence within the bone marrow niche. *Stem Cells* **35**, 1040–1052 (2017).

40. Selma, J. M. et al. Novel lipid signaling mediators for mesenchymal stem cell mobilization during bone repair. *Cell. Mol. Bioeng.* **11**, 241–253 (2018).
41. Mitchell, B. D. et al. The genetic response to short-term interventions affecting cardiovascular function: rationale and design of the Heredity and Phenotype Intervention (HAPI) Heart Study. *Am. Heart J.* **155**, 823–828 (2008).
42. The Atherosclerosis Risk in Communities (ARIC) Study: design and objectives. The ARIC investigators. *Am. J. Epidemiol.* **129**, 687–702 (1989).
43. Gottesman, O. et al. The Electronic Medical Records and Genomics (eMERGE) Network: past, present, and future. *Genet. Med.* **15**, 761–771 (2013).
44. Hughes, G. H. et al. Recruitment in the coronary artery disease risk development in young adults (cardia) study. *Control. Clin. Trials* **8**, 68S–73S (1987).
45. Fried, L. P. et al. The cardiovascular health study: Design and rationale. *Ann. Epidemiol.* **1**, 263–276 (1991).
46. Regan, E. A. et al. Genetic epidemiology of COPD (COPDGene) study design. *COPD* **7**, 32–43 (2010).
47. Splansky, G. L. et al. The third generation cohort of the national heart, lung, and Blood Institute’s Framingham Heart Study: design, recruitment, and initial examination. *Am. J. Epidemiol.* **165**, 1328–1335 (2007).
48. Becker, D. M. et al. Sex differences in platelet reactivity and response to low-dose aspirin therapy. *JAMA* **295**, 1420–1427 (2006).
49. Sorlie, P. D. et al. Design and implementation of the Hispanic Community Health Study/Study of Latinos. *Ann. Epidemiol.* **20**, 629–641 (2010).
50. Taylor, H. A. Jr et al. Toward resolution of cardiovascular health disparities in African Americans: Design and methods of the Jackson Heart Study. *Ethn. Dis.* **15**, S6–4–17 (2005).
51. Wilson, J. G. et al. Study design for genetic analysis in the Jackson Heart Study. *Ethn. Dis.* **15**, S6–30–S6–3037 (2005).
52. Bild, D. E. et al. Multi-ethnic study of atherosclerosis: Objectives and design. *Am. J. Epidemiol.* **156**, 871–881 (2002).
53. Design of the Women’s Health Initiative clinical trial and observational study. The Women’s Health Initiative Study Group. *Control. Clin. Trials* **19**, 61–109 (1998).
54. Fang, H. et al. Harmonizing genetic ancestry and self-identified race/ethnicity in genome-wide association studies. *Am. J. Hum. Genet.* **105**, 763–772 (2019).
55. Taliun, D. et al. Sequencing of 53,831 diverse genomes from the NHLBI TOPMed Program. *Nature* **590**, 290–299 (2021).
56. Regier, A. A. et al. Functional equivalence of genome sequencing analysis pipelines enables harmonized variant calling across human genetics projects. *Nat. Commun.* **9**, 4038 (2018).
57. Jeffares, D. C. et al. Transient structural variations have strong effects on quantitative traits and reproductive isolation in fission yeast. *Nat. Commun.* **8**, 14061 (2017).
58. Chiang, C. et al. SpeedSeq: Ultra-fast personal genome analysis and interpretation. *Nat. Methods* **12**, 966–968 (2015).
59. Gogarten, S. M. et al. Genetic association testing using the GENESIS R/Bioconductor package. *Bioinformatics* **35**, 5346–5348 (2019).
60. Sofer, T. et al. A fully adjusted two-stage procedure for rank-normalization in genetic association studies. *Genet. Epidemiol.* **43**, 263–275 (2019).
61. Conomos, M. P., Miller, M. B. & Thornton, T. A. Robust inference of population structure for ancestry prediction and correction of stratification in the presence of relatedness. *Genet. Epidemiol.* **39**, 276–293 (2015).
62. Pedersen, B. S. & Quinlan, A. R. Mosdepth: Quick coverage calculation for genomes and exomes. *Bioinformatics* **34**, 867–868 (2018).
63. Halko, N., Martinsson, P. G. & Tropp, J. A. Finding Structure with randomness: Probabilistic algorithms for constructing approximate matrix decompositions. *SIAM Rev.* **53**, 217–288 (2011).
64. Conomos, M. P., Reiner, A. P., Weir, B. S. & Thornton, T. A. Model-free estimation of recent genetic relatedness. *Am. J. Hum. Genet.* **98**, 127–148 (2016).
65. Lin, D.-Y. A simple and accurate method to determine genomewide significance for association tests in sequencing studies. *Genet. Epidemiol.* **43**, 365–372 (2019).
66. Kong, A. et al. Detection of sharing by descent, long-range phasing and haplotype imputation. *Nat. Genet.* **40**, 1068–1075 (2008).
67. Gudbjartsson, D. F. et al. Large-scale whole-genome sequencing of the Icelandic population. *Nat. Genet.* **47**, 435–444 (2015).
68. Loh, P.-R. et al. Efficient Bayesian mixed model analysis increases association power in large cohorts. <https://doi.org/10.1101/007799>.
69. Geoffroy, V. et al. AnnotSV: an integrated tool for structural variations annotation. *Bioinformatics* **34**, 3572–3574 (2018).
70. Sofer, T. et al. Benchmarking association analyses of continuous exposures with RNA-seq in observational studies. *Brief. Bioinform.* **22**, 1–10 (2021).
71. Shabalin, A. A. Matrix eQTL: ultra fast eQTL analysis via large matrix operations. *Bioinformatics* **28**, 1353–1358 (2012).
72. Wu, Y. et al. Highly efficient therapeutic gene editing of human hematopoietic stem cells. *Nat. Med.* **25**, 776–783 (2019).
73. Morgens, D. W. et al. Genome-scale measurement of off-target activity using Cas9 toxicity in high-throughput screens. *Nat. Commun.* **8**, 15178 (2017).
74. Li, D., Hsu, S., Purushotham, D., Sears, R. L. & Wang, T. WashU epigenome browser update 2019. *Nucleic Acids Res.* **47**, W158–W165 (2019).
75. Martin, J. S. et al. HUGIn: Hi-C unifying genomic interrogator. *Bioinformatics* **33**, 3793–3795 (2017).
76. Rao, S. S. P. et al. A 3D map of the human genome at kilobase resolution reveals principles of chromatin looping. *Cell* **159**, 1665–1680 (2014).

Acknowledgements

Molecular data for the Trans-Omics in Precision Medicine (TOPMed) program was supported by the National Heart, Lung and Blood Institute (NHLBI). See the TOPMed Omics Support Table (Supplementary Data 6) for study specific omics support information. Core support including centralized genomic read mapping and genotype calling, along with variant quality metrics and filtering were provided by the TOPMed Informatics Research Center (3R01HL-117626-02S1; contract HHSN268201800002I). Core support including phenotype harmonization, data management, sample-identity QC, and general program coordination were provided by the TOPMed Data Coordinating Center (R01HL-120393; U01HL-120393; contract HHSN268201800001I). We gratefully acknowledge the studies and participants who provided biological samples and data for TOPMed. A list of all members of the NHLBI TOPMed consortium can be found in the Supplementary Information. Genetics of Cardiometabolic Health in the Amish (Amish) The TOPMed component of the Amish Research Program was supported by NIH grants R01 HL121007, U01 HL072515, and R01 AG18728. Atherosclerosis Risk in Communities Study (ARIC) study Whole genome sequencing (WGS) for the Trans-Omics in Precision Medicine (TOPMed) program was supported by the National Heart, Lung and Blood Institute (NHLBI). WGS for “NHLBI TOPMed: Atherosclerosis Risk in Communities (ARIC)” (pfs001211) was performed at the Baylor College of Medicine Human Genome Sequencing Center (HHSN268201500015C and 3U54HG003273-12S2) and the Broad Institute for MIT and Harvard (3R01HL092577-06S1). Centralized read mapping and genotype calling, along with variant quality metrics and filtering were provided by the TOPMed Informatics Research Center (3R01HL-117626-02S1). Phenotype

harmonization, data management, sample-identity QC, and general study coordination, were provided by the TOPMed Data Coordinating Center (3R01HL-120393-02S1). We gratefully acknowledge the studies and participants who provided biological samples and data for TOPMed. The Genome Sequencing Program (GSP) was funded by the National Human Genome Research Institute (NHGRI), the National Heart, Lung, and Blood Institute (NHLBI), and the National Eye Institute (NEI). The GSP Coordinating Center (U24 HG008956) contributed to cross-program scientific initiatives and provided logistical and general study coordination. The Centers for Common Disease Genomics (CCDG) program was supported by NHGRI and NHLBI, and whole genome sequencing was performed at the Baylor College of Medicine Human Genome Sequencing Center (UM1 HG008898 and R01HL059367). The Atherosclerosis Risk in Communities study has been funded in whole or in part with Federal funds from the National Heart, Lung, and Blood Institute, National Institutes of Health, Department of Health and Human Services (contract numbers HHSN268201700001I, HHSN268201700002I, HHSN268201700003I, HHSN268201700004I and HHSN268201700005I). The authors thank the staff and participants of the ARIC study for their important contributions. Mount Sinai BioMe Biobank (BioMe) The Mount Sinai BioMe Biobank has been supported by The Andrea and Charles Bronfman Philanthropies and in part by Federal funds from the NHLBI and NHGRI (U01HG00638001; U01HG007417; X01HL134588). We thank all participants in the Mount Sinai Biobank. We also thank all our recruiters who have assisted and continue to assist in data collection and management and are grateful for the computational resources and staff expertise provided by Scientific Computing at the Icahn School of Medicine at Mount Sinai. Coronary Artery Risk Development in Young Adults (CARDIA) The Coronary Artery Risk Development in Young Adults Study (CARDIA) is conducted and supported by the National Heart, Lung, and Blood Institute (NHLBI) in collaboration with the University of Alabama at Birmingham (HHSN268201800005I & HHSN268201800007I), Northwestern University (HHSN268201800003I), University of Minnesota (HHSN268201800006I), and Kaiser Foundation Research Institute (HHSN268201800004I). CARDIA was also partially supported by the Intramural Research Program of the National Institute on Aging (NIA) and an intra-agency agreement between NIA and NHLBI (AG0005). Cardiovascular Health Study (CHS) Cardiovascular Health Study: This research was supported by contracts HHSN268201200036C, HHSN268200800007C, HHSN268201800001C, N01HC55222, N01HC85079, N01HC85080, N01HC85081, N01HC85082, N01HC85083, N01HC85086, 75N92021D00006, and grants U01HL080295 and U01HL130114 from the National Heart, Lung, and Blood Institute (NHLBI), with additional contribution from the National Institute of Neurological Disorders and Stroke (NINDS). Additional support was provided by R01AG023629 from the National Institute on Aging (NIA). A full list of principal CHS investigators and institutions can be found at CHS-NHLBI.org. The content is solely the responsibility of the authors and does not necessarily represent the official views of the National Institutes of Health. Genetic Epidemiology of COPD Study (COPDGene) The COPDGene project described was supported by Award Number U01 HL089897 and Award Number U01 HL089856 from the National Heart, Lung, and Blood Institute. The content is solely the responsibility of the authors and does not necessarily represent the official views of the National Heart, Lung, and Blood Institute or the National Institutes of Health. The COPDGene project is also supported by the COPD Foundation through contributions made to an Industry Advisory Board comprised of AstraZeneca, Boehringer Ingelheim, GlaxoSmithKline, Novartis, Pfizer, Siemens and Sunovion. A full listing of COPDGene investigators can be found at: <http://www.copdgene.org/directory> Framingham Heart Study (FHS) The Framingham Heart Study (FHS) acknowledges the support of contracts NO1-HC-25195,

HHSN268201500001I and 75N92019D00003I from the National Heart, Lung and Blood Institute and grant supplement R01 HL092577-06S1 for this research. We also acknowledge the dedication of the FHS study participants without whom this research would not be possible. Dr. Vasani is supported in part by the Evans Medical Foundation and the Jay and Louis Coffman Endowment from the Department of Medicine, Boston University School of Medicine. Genetic Studies of Atherosclerosis Risk (GeneSTAR) WGS for “NHLBI TOPMed: GeneSTAR (Genetic Study of Atherosclerosis Risk)” (phs001218) was performed at the Broad Institute of MIT and Harvard (HHSN268201500014 C), at PsomaGen (formerly MacroGen, HHSN268201500014C), and at Illumina (HL112064). GeneSTAR was supported by the National Institutes of Health/National Heart, Lung, and Blood Institute (U01 HL72518, HL087698, HL112064) and by a grant from the National Institutes of Health/National Center for Research Resources (M01-RR000052) to the Johns Hopkins General Clinical Research Center. Hispanic Community Health Study - Study of Latinos (HCHS_SOL) The Hispanic Community Health Study/Study of Latinos is a collaborative study supported by contracts from the National Heart, Lung, and Blood Institute (NHLBI) to the University of North Carolina (HHSN268201300001I / N01-HC-65233), University of Miami (HHSN268201300004I / N01-HC-65234), Albert Einstein College of Medicine (HHSN268201300002I / N01-HC-65235), University of Illinois at Chicago – HHSN268201300003I / N01-HC-65236 Northwestern Univ), and San Diego State University (HHSN268201300005I / N01-HC-65237). The following Institutes/Centers/Offices have contributed to the HCHS/SOL through a transfer of funds to the NHLBI: National Institute on Minority Health and Health Disparities, National Institute on Deafness and Other Communication Disorders, National Institute of Dental and Craniofacial Research, National Institute of Diabetes and Digestive and Kidney Diseases, National Institute of Neurological Disorders and Stroke, NIH Institution-Office of Dietary Supplements. Jackson Heart Study (JHS) The Jackson Heart Study (JHS) is supported and conducted in collaboration with Jackson State University (HHSN268201300049C and HHSN268201300050C), Tougaloo College (HHSN268201300048C), and the University of Mississippi Medical Center (HHSN268201300046C and HHSN268201300047C) contracts from the National Heart, Lung, and Blood Institute (NHLBI) and the National Institute for Minority Health and Health Disparities (NIMHD). The authors also wish to thank the staff and participants of the JHS. Multi-Ethnic Study of Atherosclerosis (MESA) Whole genome sequencing (WGS) for the Trans-Omics in Precision Medicine (TOPMed) program was supported by the National Heart, Lung and Blood Institute (NHLBI). WGS for “NHLBI TOPMed: Multi-Ethnic Study of Atherosclerosis (MESA)” (phs001416.v1.p1) was performed at the Broad Institute of MIT and Harvard (3U54HG003067-13S1). Centralized read mapping and genotype calling, along with variant quality metrics and filtering were provided by the TOPMed Informatics Research Center (3R01HL-117626-02S1, contract HHSN268201800002I). Phenotype harmonization, data management, sample-identity QC, and general study coordination, were provided by the TOPMed Data Coordinating Center (3R01HL-120393; U01HL-120393; contract HHSN268180001I). The MESA project is conducted and supported by the National Heart, Lung, and Blood Institute (NHLBI) in collaboration with MESA investigators. Support for MESA is provided by contracts 75N92020D00001, HHSN268201500003I, N01-HC-95159, 75N92020D00005, N01-HC-95160, 75N92020D00002, N01-HC-95161, 75N92020D00003, N01-HC-95162, 75N92020D00006, N01-HC-95163, 75N92020D00004, N01-HC-95164, 75N92020D00007, N01-HC-95165, N01-HC-95166, N01-HC-95167, N01-HC-95168, N01-HC-95169, UL1-TR-000040, UL1-TR-001079, UL1-TR-001420. Also supported in part by the National Center for Advancing Translational Sciences, CTSI grant UL1TR001881, and the National Institute of Diabetes and Digestive and

Kidney Disease Diabetes Research Center (DRC) grant DK063491 to the Southern California Diabetes Endocrinology Research Center. Infrastructure for the CHARGE Consortium is supported in part by the National Heart, Lung, and Blood Institute (NHLBI) grant R01HL105756. Women's Health Initiative (WHI) The WHI program is funded by the National Heart, Lung, and Blood Institute, National Institutes of Health, U.S. Department of Health and Human Services through contracts 75N92021D00001, 75N92021D00002, 75N92021D00003, 75N92021D00004, 75N92021D00005. M.M.W. was supported by a fellowship from the NHLBI BioData Catalyst program (award 1OT3HL142479-01, 1OT3HL142478-01, 1OT3HL142481-01, 1OT3HL142480-01, 1OT3HL147154). D.E.B. was supported by NHLBI DP2HL137300, R01HL130733, R01HL150553. Y.L. and J.W. were partially supported by U01HG011720 and R01HL129132. N.P. and J.L. were partially supported by R01HL154385. A.P.R. was partially supported by R01 HL146500 and R01 HL130733. We thank S.A. Wolfe for sharing 3xNLS-SpCas9 protein; R. Mathieu and the HSCI-BCH Flow Cytometry Facility, supported by the Harvard Stem Cell Institute and the NIH (U54DK110805) for assistance with flow cytometry; Fred Hutchinson Cancer Research Center, Seattle, Washington for CD34 + HSPCs (supported by Cooperative Centers of Excellence in Hematology NIDDK Grant U54DK106829). The views expressed in this manuscript are those of the authors and do not necessarily represent the views of the National Heart, Lung, and Blood Institute; the National Institutes of Health; or the U.S. Department of Health and Human Services.

Author contributions

M.M.W., D.Ba., P.L.A., and A.Re. designed the study. S.Ra., Y.Y., and D.Ba. performed experiments. M.M.W., A.M.S., B.V.H., D.Be., J.W., A.V.M., C.P.M., J.L., N.D.P., M.J., L.M.R., G.J., F.J.S., T.W.B., and P.L.A., performed data analysis. B.V.H., D.Be., U.P., M.K.M., and K.S. contributed data from deCODE genetics. J.P.L. and B.D.M. contributed data from the Amish study. P.S.V., A.C.M., and E.B. contributed data from the ARIC study. N.C., R.J.F.L., and M.P. contributed data from the BioMe biobank. M.F. and N.D.P. contributed data from the CARDIA study. J.Bi., J.S.F., and B.M.P. contributed data from the CHS study. M.H.C. and W.K. contributed data from the COPDGene study. A.D.J. contributed data from the FHS study. L.C.B., L.R.Y., K.K., and R.A.M. contributed data from the GeneSTAR study. J.M. and R.C.K. contributed data from the HCHS/SOL study. Y.G., L.M.R., and Y.L. contributed data from the JHS study. A.Ra., S.Ri., J.I.R., and R.P.T. contributed data from the MESA study. P.D., H.T., and A.Re. contributed data from the WHI study. G.M., G.R.A., A.V.S., D.A.N., M.P.C., D.Ba., P.L.A., and A.Re. jointly supervised the research.

M.M.W., A.M.S., D.Ba., P.L.A., and A.Re. drafted the manuscript. J.Bl., L.A., and J.E.C. reviewed the manuscript. All authors reviewed the manuscript and provided critical revision.

Competing interests

G.R.A. is an employee of Regeneron Pharmaceuticals; he owns stock and stock option for Regeneron Pharmaceuticals. L.M.R. is a consultant for the TOPMed Administrative Coordinating Center (through WeStat). The remaining authors declare no competing interests.

Additional information

Supplementary information The online version contains supplementary material available at <https://doi.org/10.1038/s41467-022-35354-7>.

Correspondence and requests for materials should be addressed to Paul L. Auer or Alex P. Reiner.

Peer review information *Nature Communications* thanks the anonymous reviewers for their contribution to the peer review of this work.

Reprints and permissions information is available at <http://www.nature.com/reprints>

Publisher's note Springer Nature remains neutral with regard to jurisdictional claims in published maps and institutional affiliations.

Open Access This article is licensed under a Creative Commons Attribution 4.0 International License, which permits use, sharing, adaptation, distribution and reproduction in any medium or format, as long as you give appropriate credit to the original author(s) and the source, provide a link to the Creative Commons license, and indicate if changes were made. The images or other third party material in this article are included in the article's Creative Commons license, unless indicated otherwise in a credit line to the material. If material is not included in the article's Creative Commons license and your intended use is not permitted by statutory regulation or exceeds the permitted use, you will need to obtain permission directly from the copyright holder. To view a copy of this license, visit <http://creativecommons.org/licenses/by/4.0/>.

© The Author(s) 2022

Marsha M. Wheeler^{1,40}, Adrienne M. Stilp^{2,40}, Shuquan Rao^{3,4,5,6,7,8,40}, Bjarni V. Halldórsson^{9,10}, Doruk Beyter⁹, Jia Wen¹¹, Anna V. Mihkaylova², Caitlin P. McHugh², John Lane¹², Min-Zhi Jiang¹¹, Laura M. Raffield¹³, Goo Jun¹⁴, Fritz J. Sedlazeck¹⁵, Ginger Metcalf¹⁵, Yao Yao^{3,4,5,6,7}, Joshua B. Bis¹⁶, Nathalie Chami¹⁷, Paul S. de Vries^{14,18}, Pinkal Desai¹⁹, James S. Floyd¹⁶, Yan Gao²⁰, Kai Kammers²¹, Wonji Kim²², Jee-Young Moon²³, Aakrosh Ratan²⁴, Lisa R. Yanek²¹, Laura Almasy²⁵, Lewis C. Becker²¹, John Blangero²⁶, Michael H. Cho²², Joanne E. Curran²⁶, Myriam Fornage²⁷, Robert C. Kaplan²³, Joshua P. Lewis²⁸, Ruth J. F. Loos^{17,29,30,31}, Braxton D. Mitchell²⁸, Alanna C. Morrison¹⁸, Michael Preuss¹⁷, Bruce M. Psaty¹⁶, Stephen S. Rich²⁴, Jerome I. Rotter³², Hua Tang³³, Russell P. Tracy³⁴, Eric Boerwinkle¹⁸, Goncalo R. Abecasis³⁵, Thomas W. Blackwell³⁵, Albert V. Smith³⁵, Andrew D. Johnson³⁶, Rasika A. Mathias²¹, Deborah A. Nickerson^{1,41}, Matthew P. Conomos², Yun Li¹¹, Unnur Porsteinsdóttir^{9,37}, Magnús K. Magnússon^{9,37}, Kari Stefansson^{9,37}, Nathan D. Pankratz^{12,40}, Daniel E. Bauer^{3,4,5,6,7,40}, Paul L. Auer³⁸ ✉ & Alex P. Reiner³⁹ ✉

¹Department of Genome Sciences, University of Washington, Seattle, WA 98105, USA. ²Department of Biostatistics, University of Washington, Seattle, WA 98105, USA. ³Division of Hematology/Oncology, Boston Children's Hospital, Boston, MA 02115, USA. ⁴Department of Pediatric Oncology, Dana-Farber Cancer Institute, Boston, MA 02115, USA. ⁵Harvard Stem Cell Institute, Boston, MA 02138, USA. ⁶Broad Institute, Cambridge, MA 02142, USA. ⁷Department of Pediatrics, Harvard Medical School, Boston, MA 02115, USA. ⁸State Key Laboratory of Experimental Hematology, National Clinical Research Center for Blood

Diseases, Haihe Laboratory of Cell Ecosystem, Institute of Hematology & Blood Diseases Hospital, Chinese Academy of Medical Sciences & Peking Union Medical College, Tianjin 300020, China. ⁹deCODE genetics/Amgen Inc., Reykjavik, Iceland. ¹⁰School of Technology, Reykjavik University, Reykjavik, Iceland. ¹¹Departments of Biostatistics, Genetics, Computer Science, Applied Physical Sciences, University of North Carolina at Chapel Hill, Chapel Hill, NC 27599, USA. ¹²Department of Laboratory Medicine and Pathology, University of Minnesota Medical School, Minneapolis, MN 55455, USA. ¹³Department of Genetics, University of North Carolina, Chapel Hill, NC 27599, USA. ¹⁴Human Genetics Center, School of Public Health, The University of Texas Health Science Center at Houston, Houston, TX 77030, USA. ¹⁵Human Genome Sequencing Center, Baylor College of Medicine, Houston, TX, USA. ¹⁶Cardiovascular Health Research Unit, Department of Medicine, University of Washington, Seattle, WA 98101, USA. ¹⁷The Charles Bronfman Institute for Personalized Medicine, Icahn School of Medicine at Mount Sinai, New York, NY 10029, USA. ¹⁸Department of Epidemiology, Human Genetics, and Environmental Sciences, School of Public Health, The University of Texas Health Science Center at Houston, Houston, TX 77030, USA. ¹⁹Division of Hematology and Oncology, Weill Cornell Medical College, New York, NY 10065, USA. ²⁰Jackson Heart Study, Department of Medicine, University of Mississippi, Jackson, MS 39216, USA. ²¹GeneSTAR Research Program, Department of Medicine, Johns Hopkins University School of Medicine, Baltimore, MD 21287, USA. ²²Channing Division of Network Medicine, Brigham and Women's Hospital, Boston, MA 2115, USA. ²³Department of Epidemiology and Population Health, Albert Einstein College of Medicine, Bronx, NY 10461, USA. ²⁴Center for Public Health Genomics, University of Virginia, Charlottesville, VA 22908, USA. ²⁵Children's Hospital of Philadelphia and University of Pennsylvania School of Medicine, Philadelphia, PA 19104, USA. ²⁶Department of Human Genetics and South Texas Diabetes and Obesity Institute, University of Texas Rio Grande Valley School of Medicine, Brownsville, TX 78520, USA. ²⁷Brown Foundation Institute of Molecular Medicine, McGovern Medical School, University of Texas Health Science Center at Houston, Houston, TX 77030, USA. ²⁸Department of Medicine, Division of Endocrinology, Diabetes, and Nutrition, University of Maryland School of Medicine, Baltimore, MD, USA. ²⁹Department of Environmental Medicine and Public Health, Icahn School of Medicine at Mount Sinai, New York, NY, USA. ³⁰The Mindich Child Health and Development Institute, Icahn School of Medicine at Mount Sinai, New York, NY, USA. ³¹Novo Nordisk Foundation Center for Basic Metabolic Research, Faculty of Health and Medical Sciences, University of Copenhagen, Copenhagen, Denmark. ³²The Institute for Translational Genomics and Population Sciences, Department of Pediatrics, The Lundquist Institute for Biomedical Innovation at Harbor-UCLA Medical Center, Torrance, CA 90502, USA. ³³Department of Genetics, Stanford University School of Medicine, Stanford, CA 94305, USA. ³⁴Departments of Pathology & Laboratory Medicine and Biochemistry, Larner College of Medicine at the University of Vermont, Colchester, VT 5446, USA. ³⁵TOPMed Informatics Research Center, University of Michigan, Department of Biostatistics, Ann Arbor, MI 48109, USA. ³⁶Population Sciences Branch, Division of Intramural Research, National Heart, Lung and Blood Institute, Framingham, MA 1702, USA. ³⁷Faculty of Medicine, University of Iceland, 101 Reykjavik, Iceland. ³⁸Division of Biostatistics, Institute for Health and Equity, and Cancer Center, Medical College of Wisconsin, Milwaukee, WI 53226, USA. ³⁹Department of Epidemiology, University of Washington, Seattle, WA 98105, USA. ⁴⁰These authors contributed equally: Marsha M. Wheeler, Adrienne M. Stilp, Shuquan Rao, Nathan D. Pankratz, Daniel E. Bauer. ⁴¹Deceased: Deborah A. Nickerson. ✉e-mail: pauer@mcw.edu; apreiner@uw.edu